15486

WT-1311 (EX)

EXTRACTED VERSION

# OPERATION REDWING

## Project 2.2
## Gamma Exposure Rate Versus Time

Pacific Proving Grounds
May – July 1956

Headquarters Field Command
Defense Atomic Support Agency
Sandia Base, Albuquerque, New Mexico

January 18, 1960

NOTICE

This is an extract of WT-1311, Operation REDWING, Project 2.2, which remains classified SECRET/FORMERLY RESTRICTED DATA as of this date.

Extract version prepared for:

Director
DEFENSE NUCLEAR AGENCY
Washington, D.C. 20305

15 May 1981

**Approved for public release; distribution unlimited.**

SUMMARY OF SHOT DATA, OPERATION REDWING

| Shot Name (Unclassified) | Date (PPG) | Time (Approximate) | Location | Type | H&N Coordinates (Actual Ground Zero) | Geographic |
|---|---|---|---|---|---|---|
| | | | | | | ° ' " |
| Lacrosse | 5 May | 0629 | Eniwetok<br>Yvonne | Surface<br>Land | 124515 E<br>106885 N | 11 33 29<br>162 21 18 |
| Cherokee | 21 May | 0551 | Bikini<br>Off Charlie | Air Drop<br>Over Water | 96200 ± 100 E<br>185100 ± 500 N | 11 43 50<br>165 19 46 |
| Zuni | 28 May | 0556 | Bikini<br>Tare | Surface<br>Land Water | 110309 E<br>100154 N | 11 29 48<br>165 22 09 |
| Yuma | 28 May | 0756 | Eniwetok<br>Sally | 200-ft Tower | 112155 E<br>130604 N | 11 37 24<br>162 19 13 |
| Erie | 31 May | 0615 | Eniwetok<br>Yvonne | 300-ft Tower | 127930 E<br>[illegible] N | 11 32 41<br>162 21 52 |
| Seminole | 6 June | 1255 | Eniwetok<br>Irene | Surface<br>Land[a] | 75537 E<br>149897 N | 11 40 35<br>162 13 02 |
| Flathead | 12 June | 0626 | Bikini<br>Off Dog | Barge<br>Water | 116768 E<br>164094 N | 11 40 22<br>165 23 13 |
| Blackfoot | 12 June | 0626 | Eniwetok<br>Yvonne | 200-ft Tower | 126080 E<br>104435 N | 11 33 04<br>162 21 33 |
| Kickapoo | 14 June | 1126 | Eniwetok<br>Sally | 300-ft Tower | 114018 E<br>132295 N | 11 37 41<br>162 19 32 |
| Osage | 16 June | 1314 | Eniwetok<br>Yvonne | Air Drop<br>Over Land | 126627 ± 50 E<br>102851 ± 50 N | 11 32 48<br>162 21 39 |
| Inca | 22 June | 0956 | Eniwetok<br>Pearl | 200-ft Tower | 105300 E<br>133540 N | 11 37 53<br>162 18 04 |
| Dakota | 26 June | 0606 | Bikini<br>Off Dog | Barge<br>Water | 116767 E<br>164097 N | 11 40 22<br>165 23 13 |
| Mohawk | 3 July | 0606 | Eniwetok<br>Ruby | 300-ft Tower | 109737 E<br>132165 N | 11 37 39<br>162 18 49 |
| Apache | 9 July | 0606 | Eniwetok<br>Flora | Barge<br>Water | 69227 E<br>148063 N | 11 40 17<br>162 12 01 |
| Navajo | 11 July | 0556 | Bikini<br>Off Dog | Barge<br>Water | 116816 E<br>160604 N | 11 39 48<br>165 23 14 |
| Tewa | 21 July | 0546 | Bikini<br>Charlie-Dog Reef | Barge<br>Water | 99776 E<br>164476 N | 11 40 26<br>165 20 22 |
| Huron | 22 July | 0616 | Eniwetok<br>Flora | Barge<br>Water | 70015 E<br>148304 N | 11 40 19<br>162 12 09 |

[a]See ITR-1344 for further details.

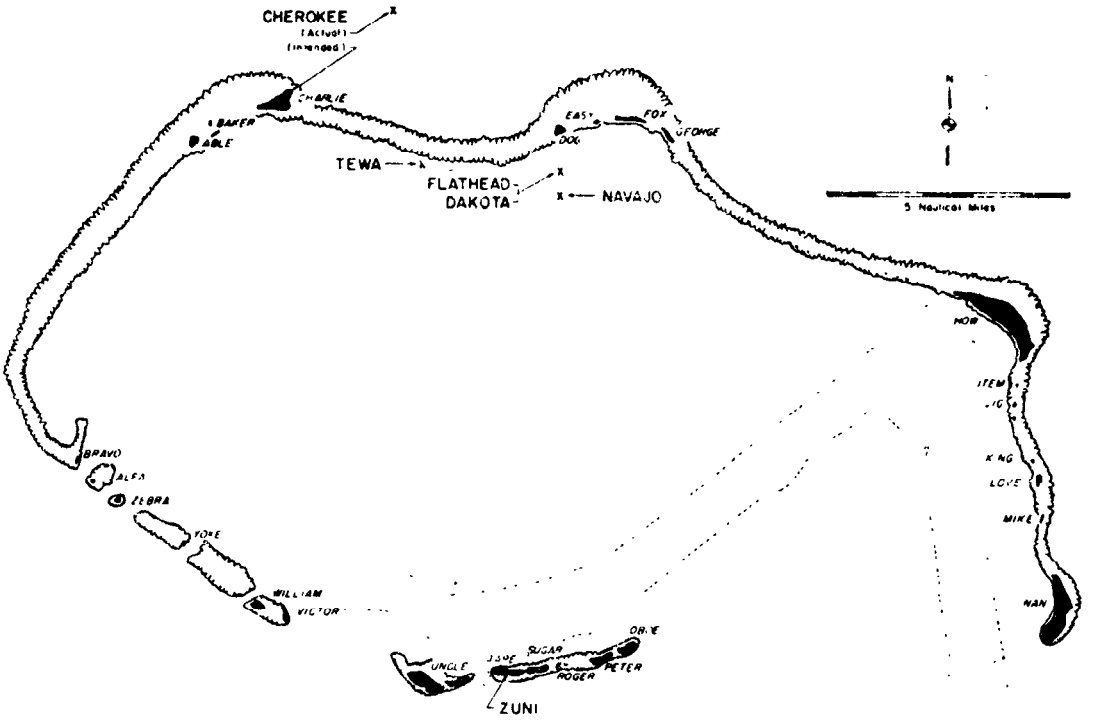


| | | | | | | | |
|---|---|---|---|---|---|---|---|
| Airukiiji | Oboe | Bokoaetokutoku | Alfa | Enlirikku | Uncle | Rochikarai | Love |
| Airukiraru | Peter | Bokobyaadaa | Able | Enlnman | Tare | Romurikku | Fox |
| Aomoen | George | Bokonejien | Baker | Enyu | Nan | Rukoji | Victor |
| Arrilkan | Yoke | Bokonfuaaku | Item | Ionchebi | Mike | Uorikku | Easy |
| Bigiren | Roger | Bokororyuru | Bravo | Namu | Charley | Yomyaran | Jig |
| Bikini | How | Chieerete | William | Ourukaen | Zebra | Yurochi | Dog |
| | | Enlairo | King | Reere | Sugar | | |

Bikini Atoll. Locations of test detonations during Operation Redwing are indicated by large lettering and arrows. Native island names with corresponding military identifiers are given in the tabulation.

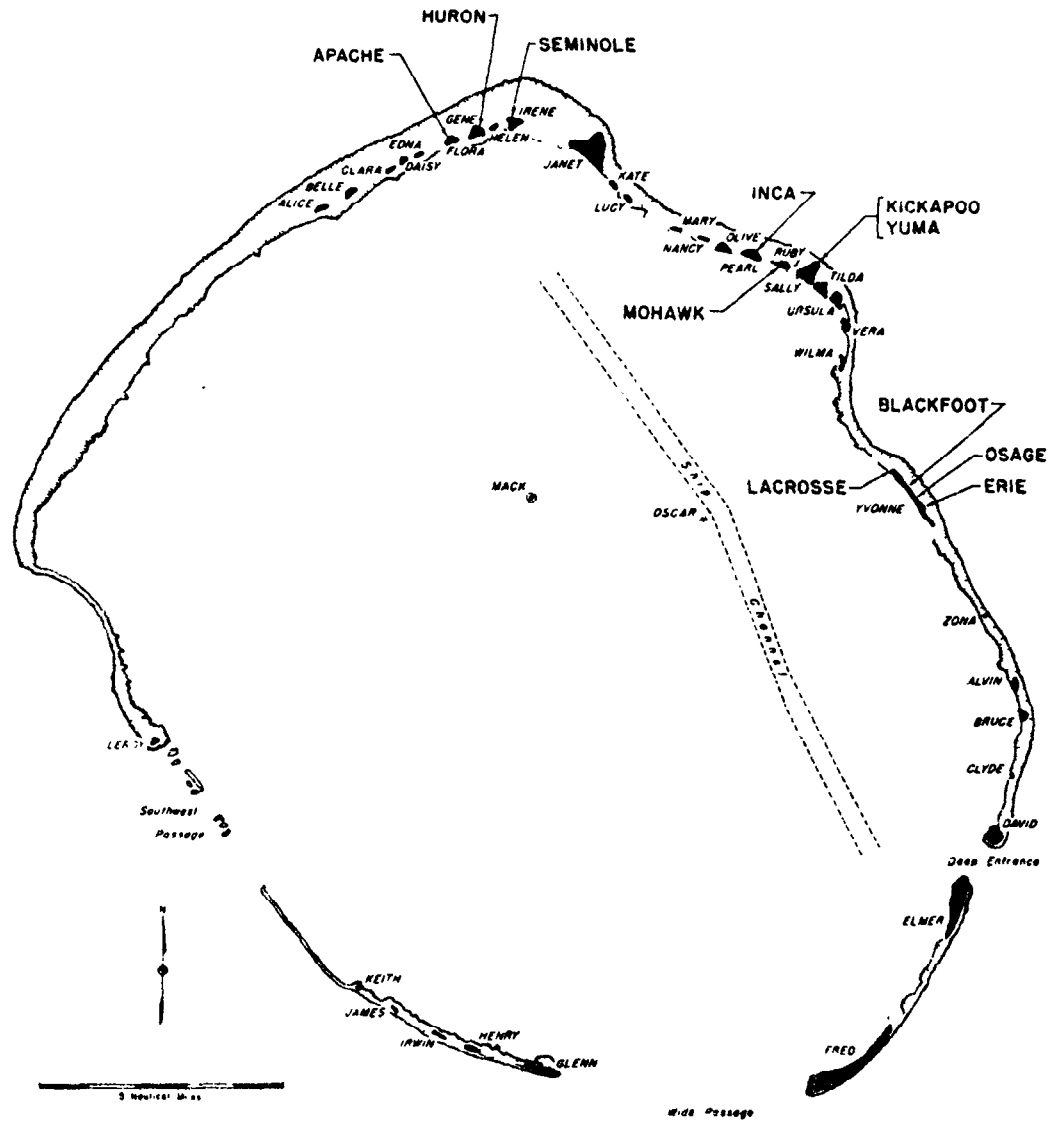


| | | | | | | | |
|---|---|---|---|---|---|---|---|
| Aaraanbiru | Vera | Chinieero | Alvin | Igurin | Glenn | Ribaion | James |
| Aitsu | Olive | Chinimi | Clyde | Japtan | David | Rigili | Leroy |
| Aniyaanii | Bruce | Cochita | Daisy | Kirinian | Lucy | Rojoa | Ursula |
| Aomon | Sally | Coral Heads | Mack, Oscar | "M" | Zona | Ruchi | Clara |
| Bijiri | Tilda | Eberiru | Ruby | Mai | Henry | Rujoru | Pearl |
| Bogairikk | Helen | Elugelab | Flora | Muzin | Kate | Runit | Yvonne |
| Bogallua | Alice | Engebi | Janet | Parry | Elmer | Sandildefonso | Edna |
| Bogombogo | Belle | Eniwetok | Fred | Pliraai | Wilma | Teiteiripucchi | Gene |
| Bogon | Irene | Giriinien | Keith | Pokon | Irwin | Yeiri | Nancy |
| Eokonaarappu | Mary | | | | | | |

Eniwetok Atoll. Locations of test detonations during Operation Redwing are indicated by large lettering and arrows. Native island names with corresponding military identifiers are given in the tabulation.

# ABSTRACT

The primary objective of Project 2.2 was to measure initial- and residual-gamma-exposure rates as a function of time at various distances from high-yield-thermonuclear detonations. Secondary objectives were to measure the residual gamma-exposure rate at the lip of the crater from a high-yield, land-surface shot; and to field test a prototype thermal detector to be used in a radiological-defense-warning system.

The residual-gamma radiation was detected by an unsaturated-ion chamber, whose output determined the frequency of pulses that were recorded on electro-sensitive paper. Most of the initial-gamma-radiation stations consisted of scintillation detectors whose output determined the frequency of pulses that were recorded on magnetic tape. Some initial-gamma instruments were similar to those used during Operation Castle. The exposure rate near the crater was measured with a detector-telemeter unit dropped from a helicopter.

Residual-gamma-exposure rate versus time was obtained after Shots Zuni, Flathead, Navajo, and Tewa. The observed average-decay exponents for these events were 1.1 for Zuni and Tewa, 1.2 for Flathead, and 1.3 for Navajo. In some cases, the effect of rainfall in leaching the activity decreased the exposure rate by a factor of two.

Records from Shot Flathead at 7,730 feet and from Shot Navajo at 13,870 feet indicated that at these locations about $^2/_3$ of the total initial-gamma exposure was delivered after the arrival of the shock front.

The crater-lip measurements indicated that the method was a feasible one; however, no usable data was obtained.

The thermal-radiation detector responded satisfactority to a detonation at a distance of 20 miles.

# FOREWORD

This report presents the final results of one of the projects participating in the military-effect programs of Operation Redwing. Overall information about this and the other military-effect projects can be obtained from WT – 1344, the "Summary Report of the Commander, Task Unit 3." This technical summary includes: (1) tables listing each detonation with its yield, type, environment, meteorological conditions, etc.; (2) maps showing shot locations; (3) discussions of results by programs; (4) summaries of objectives, procedures, results, etc., for all projects; and (5) a listing of project reports for the military-effect programs.

# CONTENTS

FIGURES

TABLES

# Chapter 1
# INTRODUCTION

## 1.1 OBJECTIVES

The primary objectives of Project 2.2 were: (1) to measure the initial-gamma-exposure rate as a function of time from the detonation of high-yield-thermonuclear devices; and (2) to measure the residual-gamma-exposure rate as a function of time at land fallout stations. Secondary objectives were: (1) to measure residual radiation at early times on the crater lip of a high-yield, land-surface shot; and (2) to field test a prototype thermal-radiation detector to be used in a radiological-defense-warning system.

## 1.2 BACKGROUND

Los Alamos Scientific Laboratory (LASL) measured initial-gamma-exposure rate versus time for high-yield devices during Operation Ivy (Reference 1). It was found that high-yield devices did not follow the relatively simple scaling laws of low-yield devices. Gamma radiation at a particular distance scales linearly with yield for devices up to about 100 kt. For megaton-range devices, gamma radiation scales higher with increasing yield. This enhancement of initial-gamma radiation was attributed largely to the hydrodynamic effect (Section 1.3.4). U. S. Army Signal Research and Development Laboratory (USASRDL) obtained several gamma-exposure-rate-versus-time data points from high-yield devices during Operation Castle (Reference 2). The data obtained by USASRDL were lower by a factor of 10 or more than the Super-Effects Handbook predictions (Reference 3).

One of the purposes of Project 2.2 was to resolve the initial-gamma-radiation-scaling laws for high-yield devices. Of particular interest was a high-yield air burst, since it would allow correlation of the hydrodynamic effect from an airburst with that from a surface burst. USASRDL made measurements of residual-gamma-exposure rates from high-yield devices during Operation Castle (Reference 2). Only limited data were obtained because of a high loss of instruments early in the operation. These data indicated that the decay exponent for the residual activity varied with the type of nuclear device. Another purpose of Project 2.2 was to determine accurate decay exponents for residual activity.

The thermal-radiation detector, part of an early-warning system for nuclear detonations, was tested with low-yield devices during Operation Teapot (Reference 4). The tests were successful. The detector showed a capability far in excess of the requirements. It was decided to determine the response of this detector to megaton-range devices during Operation Redwing in order to complete the testing.

## 1.3 THEORY

The gamma radiation emitted from a nuclear detonation may be divided into two por-

tions: Initial radiation and residual radiation. The residual radiation may include radiation from both fallout and neutron-induced activity.

1.3.1 Initial-Gamma Radiation. For a fission-type device the initial radiations are divided approximately as shown in Table 1.1 (from Reference 5). The major contribution to initial-gamma radiation is from the fission-product gammas and the gamma radiation from neutron capture by $N^{14}$ (n, $\gamma$) in the high-explosive components and air. The prompt gammas are nearly all absorbed in the device itself and are of little significance outside of the device. The fission-product gammas predominate at close distances (Reference 5). The $N^{14}$ (n, $\gamma$) gammas become relatively more important at greater distances, and eventually become the major contributor. This applies only to devices with yields of less than 100 kt, in which the hydrodynamic effect is small. Figure 1.1 shows the contribution

TABLE 1.1 ENERGY PARTITION IN FISSION

| Mechanism | Percent of Total Fission Energy | Total Energy per Fission |
|---|---|---|
| | pct | Mev |
| Kinetic Energy of Fission Fragments | 81.0 | 162.0 |
| Prompt Neutrons | 4.0 | 8.0 |
| Prompt Gammas* | 4.0 | 8.0 |
| Fission Product Gammas | 2.7 | 5.4 |
| Fission Product Betas | 2.7 | 5.4 |
| Fission Product Neutrinos | 5.5 | 11.0 |
| Delayed Neutrons | 0.1 | 0.2 |
| Totals | 100.0 | 200.0 |

* Mostly absorbed in the device.

from fission-product gammas and $N^{14}$ (n, $\gamma$) for a one-kt surface burst. With respect to time, the $N^{14}$ (n, $\gamma$) radiation is essentially emitted within 0.2 second; the fission-product gammas, however, continue to contribute for the first 30 seconds.

For thermonuclear devices, in addition to gamma radiation from fission-product gammas, it is necessary to consider the interaction of neutrons from the fusion process with $N^{14}$. The radiation due to the fusion process may vary over wide limits, depending on the design of the device. For a given yield, the number of neutrons available may be ten times as great for fusion as for fission, and therefore a large contribution to gamma-radiation exposure may be due to the $N^{14}$ (n, $\gamma$) reaction in a thermonuclear device (Reference 3).

1.3.2 Residual-Gamma Radiation. Residual-gamma radiation consists of fission-product radiation from fallout and radiation from neutron-induced activity. The decay rate of the residual radiation from fallout will follow approximately the expressions:

$$I_t = I_1 t^{-1.2}$$

and:

$$r = \int_{t_1}^{t_2} I_t \, dt = 5 I_1 (t_1^{-0.2} - t_2^{-0.2}) \qquad (1.1)$$

Where: $I_t$ = exposure rate at time t

$I_1$ = exposure rate at unit time

t = time

r = exposure between times $t_1$ and $t_2$, where $t_1 \geq 10$ seconds

The decay of the residual radiation is expected to vary with device design. For example, the presence of $Np^{239}$ would tend to decrease the absolute value of the decay exponent for a period of time.

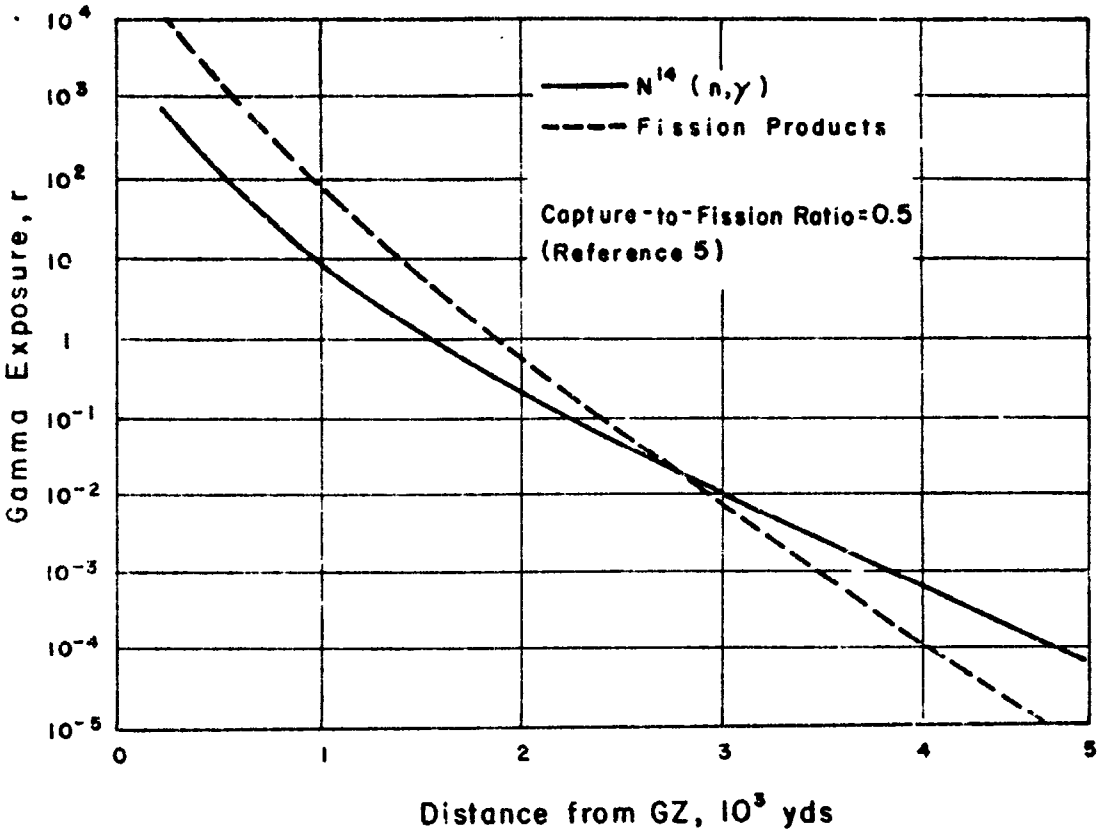


Figure 1.1 Graph of gamma exposure versus distance for a one kt surface burst. This illustration shows the contribution from fission-product gammas.

1.3.3 Absorption in Air. The absorption of unscattered gamma radiation in air is exponential with distance. From a point source of mono-energetic radiation, the variation of intensity with distance is expressed as:

$$I_D = I_0 e^{-\mu D}/4\pi D^2 \qquad (1.2)$$

Where: $I_D$ = intensity at distance D

$I_0$ = source intensity

$\mu$ = total linear absorption coefficient (this coefficient generally decreases with increasing gamma energy)

D = distance

The absorption coefficient $\mu$ in Equation 1.2 is applicable for narrow-beam geometry, and a correction should be made for field conditions where the detector is approximately a $2\pi$ sensing element. This is done by adding a buildup factor B to Equation 1.2 to account for the scattered radiation that will be detected. Buildup factors for different energies and distances have been calculated (Reference 6), and some values are shown in Table 1.2. For omni-directional detectors, the expression is:

$$I_D = I_0 B e^{-\mu D}/4\pi D^2 \qquad (1.3)$$

1.3.4 Hydrodynamic Effect. As shown in Section 1.3.3, the attenuation of gamma radiation is highly dependent on the amount of absorber between the source and the detector. For devices of less than 100-kt yield, essentially all of the initial-gamma radiation is emitted before the shock front can produce an appreciable change in the effective

TABLE 1.2 CALCULATED BUILDUP FACTORS

The buildup factor (B) given here is the factor $B_r$ ($\mu_0 D$, $E_0$) as computed by Nuclear Development Associates for AFSWP (Reference 6).

| Energy ($E_0$) | B | | |
|---|---|---|---|
| | 1,000 | 1.500 | 3,000 |
| Mev | yds | yds | yds |
| 1 | 16.2 | 29.3 | 85.0 |
| 3 | 3.85 | 5.35 | 10.2 |
| 4 | 2.97 | 4.00 | 7.00 |
| 10 | 1.70 | 2.01 | 2.90 |

absorption of the air between source and detector. For high-yield devices, the velocity of the shock front is sufficiently high to produce a strong enhancement of a large percentage of the initial-gamma radiation (Reference 7). The higher the yield, the larger is this percentage. A simplified treatment of the hydrodynamic effect follows.

Assume a sphere that has a volume $V_0$ and radius R, and is filled with a gas of density $\rho_0$ and mass M. Then,

$$M = V_0 \rho_0 = 4\pi R^3 \rho_0/3 \qquad (1.4)$$

Let the gas be compressed into a shell with thickness $\Delta R$ (R remaining constant). The new gas volume is expressed as $V_1$ ($V_1 = 4\pi R^2 \Delta R$) with a density of $\rho_1$. The mass has not changed; thus,

$$M = V_0 \rho_0 \doteq 4\pi R^2 \Delta R \rho_1 \qquad (\Delta R \ll R)$$

$$4\pi R^3 \rho_0/3 \doteq 4\pi R^2 \Delta R \rho_1 \qquad (1.5)$$

$$\Delta R \rho_1 \doteq R\rho_0/3 \qquad (1.6)$$

Equation 1.6 indicates that a ray originating in the center of the sphere would traverse only $\frac{1}{3}$ of the mass in the shell model that it would in the homogeneous model. The result would be an enhancement of radiation. Once the shell of material in the shock front passes the detector, an even greater enhancement results.

As previously stated, the $N^{14}$ (n, $\gamma$) component of initial radiation is essentially emitted within 0.2 second. Since it takes at least one second for the shock front to reach a detector at a distance of 7,000 feet (even for devices in the order of 6 Mt), the $N^{14}$ (n, $\gamma$) component is not significantly enhances. The fission-product gammas continue to contribute during the first 30 seconds; therefore, this radiation is strongly enhanced by the shock wave.

# Chapter 2
# PROCEDURE

## 2.1 OPERATIONS

Table 2.1 lists shot participation and instrumentation. The instrument stations were placed in previously prepared positions at the latest practicable time prior to each shot and were recovered postshot as soon as Rad-Safe conditions permitted. The residual stations were activated upon placement. Their 5-day operating period allowed for 2 days of data-recording and three 1-day shot delays. For the surface bursts, the initial stations were activated by a minus-1-minute-timing signal for warmup, and a minus-15-second signal to start the recorder. Shot Zuni was an exception; only a minus-1-second signal was available to start the recorder. Timing signals were necessary on the initial stations because of the limited recording time available (Cook Research Laboratory MR 33 recorders, 4 minutes; Sanborn recorders, 15 minutes). For Shot Cherokee, the recorders were not started until after the device release.

## 2.2 INSTRUMENTATION

In designing instrumentation for this project, there were two objectives: (1) to design instruments to best fulfill the requirements; and (2) to design flexible instruments readily adaptable to a wide variety of field measurements. In view of this dual objective, the instruments were designed to be compact, drift-free, reliable, wide in dynamic-range coverage, and low in cost. The basic circuit evolved measured discrete increments of charge. Essentially, this circuit could be used with any sensing element that had an output which was a known function of the radiation field. Thus, the circuit was equally applicable to ion chambers, scintillation detectors, or photo-conductive crystals.

In operation, the charge on $C_1$ (Figure 2.1) held tube $T_1$ well beyond cutoff. The output current of the sensing element discharged $C_1$ at a rate dependent upon the radiation level. When the voltage at the grid of $T_1$ reached the grid base, $T_1$ conducted, fed a negative signal to the grid of $T_2$, and initiated a regenerative action which rapidly cut off $T_2$. Then $C_1$ charged to a potential equal to B-plus less the cathode voltage and the grid-to-cathode drop through the diode action of the grid of $T_1$. When $C_1$ was completely charged, the circuit returned to its normal condition of $T_2$ conducting and $T_1$ cutoff. The circuit remained in this condition until $C_1$ was once more discharged by the output of the sensing element. The output of this circuit consisted of pulses that had a repetition rate proportional to the output current of the sensing element.

2.2.1 The Residual Instrument System, Conrad I Detector. In general, decay of the gamma-exposure rate from fallout contamination is given by:

$$I = I_1 t^{-x} \tag{2.1}$$

Where: $I$ = the gamma-exposure rate at time $t$

$I_1$ = the gamma-exposure rate at unit time

$x$ = the decay constant (given as 1.2 for gross fission products)

TABLE 2.1 SHOT PARTICIPATION AND INSTRUMENTATION

Ig = initial station, Gustave; Ip = initial station, Photomultiplier; R = Residual station;

| Shot | Station Number | Station Location | Range from Ground Zero | Instrumentation |
|---|---|---|---|---|
| | | | ft | |
| Cherokee | 221.01 | Able | 29,400 | Ip, Ig, R |
| | 221.02 | Charlie | 20,694 | Ip, Ig, R |
| | 221.03 | Dog | 16,370 | R |
| | 221.04 | Easy | 20,062 | R |
| | 221.05 | Fox | 24,922 | R |
| | 221.06 | George | 30,207 | R |
| | 220.01C | Uncle | 85,432 | R |
| | 220.08C | Oboe | 76,310 | R |
| | 221.02C | Yoke | 63,720 | R |
| | Portable | Nan | — | R |
| Zuni | 221.03 | Dog | 68,600 | R |
| | 221.06 | George | 70,900 | R |
| | 220.01C | Uncle | 10,300 | R |
| | 220.08C | Oboe | 16,270 | Ip, R |
| | 220.09C | Roger | 7,000 | Ip, Ig, R |
| | 220.14C | Peter | 11,270 | R |
| | 221.01C | William | 10,320 | R |
| | 221.02C | Yoke | 43,400 | R |
| | 221.04 | Alfa | 56,570 | R |
| | Portable | How | 78,000 | R |
| | Portable | Love | 72,000 | R |
| | Portable | Nan | 69,000 | R |
| Flathead | 221.01 | Able | 45,800 | R |
| | 221.03 | Dog | 4,422 | Ip, Ig, R |
| | 221.04 | Easy | 7,730 | Ip, Ig, R |
| | 221.05 | Fox | 10,745 | Ip, R |
| | 221.06 | George | 14,920 | R |
| | 220.08C | Oboe | 59,800 | R |
| | 220.09C | Roger | 63,155 | R |
| | 220.14C | Peter | 62,344 | R |
| | 221.01C | William | 40,907 | R |
| | 221.02C | Yoke | 9,068 | R |
| | 221.04C | Alfa | 70,000 | R |
| | Portable | How | 60,000 | R |
| | Portable | Love | 75,000 | R |
| | Portable | Nan | 85,000 | R |
| Navajo | 221.01 | Able | 46,000 | R |
| | 221.03 | Dog | 7,922 | Ip, Ig, R |
| | 221.04 | Easy | 10,700 | Ip, R |
| | 221.05 | Fox | 13,170 | Ig, R |
| | 221.06 | George | 16,180 | Ig, R |
| | 220.08C | Oboe | 56,341 | R |
| | 220.01C | Uncle | 58,282 | R |
| | 221.01C | William | 36,006 | R |
| | 221.02C | Yoke | 15,582 | R |
| | Portable | How | 60,000 | R |
| | Portable | Love | 72,000 | R |
| | Portable | Nan | 84,000 | R |
| Tewa | 221.01 | Able | 28,950 | R |
| | 221.03 | Dog | 17,550 | Ip, Ig, R |
| | 221.04 | Easy | 22,200 | R |
| | 221.05 | Fox | 24,711 | R |
| | 220.08C | Oboe | 54,066 | R |
| | — | MM2 | 5,960 | Ig |
| | 221.01C | William | 51,775 | R |
| | 221.02C | Yoke | 37,631 | R |
| | Portable | How | 70,000 | R |

Measurements of the decay constant require good (short) time resolution at early times (t small, I large) when the changes in gamma-exposure rate are most rapid. At later times (t large, I small), the rate of change of the gamma-exposure rate of the gamma radiation is much smaller, and the instrument system need not have such good time resolution. The instrument for the measurement of residual-gamma radiation was designed to cover a range from 1 r/hr with a time resolution of 5 minutes, to $10^4$ r/hr with a time resolution of 0.05 minutes. The basic circuit is shown in Figure 2.1, where

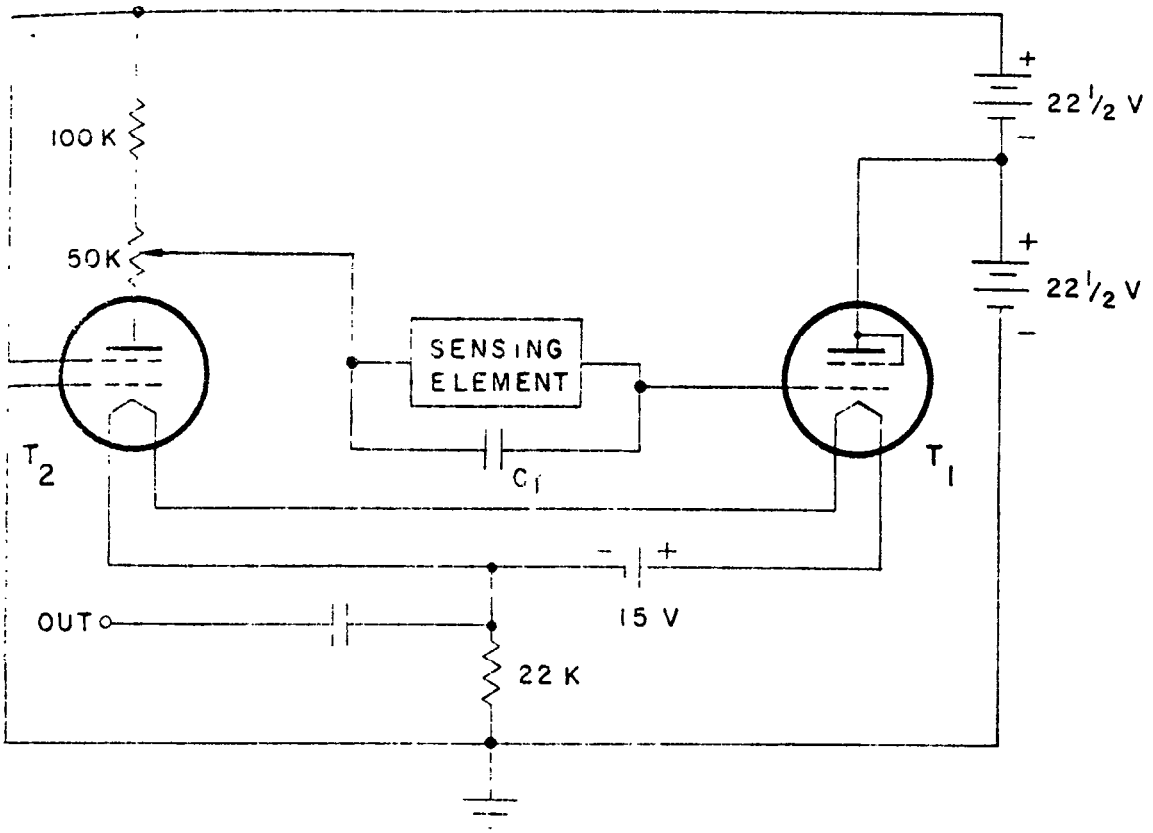


Figure 2.1 Schematic diagram showing the basic circuit for the Conrad and Gustave detectors. The Conrad detector used an unsaturated ion chamber as the sensing element, whereas the Gustave detector used a scintillation detector.

the sensing element is an unsaturated ion chamber. The ion chamber was designed to have a current output proportional to the square root of the gamma-exposure rate. The overall detector response is given by:

$$f = kr^{1/2} \tag{2.2}$$

Where: f = the output frequency

r = the gamma-exposure rate in r/hr

k = a parameter chosen to meet specific design objectives

In laboratory calibrations on a 250-kv X-ray beam, these detectors showed a preci-

sion of better than two percent, including drift effects, over a three-week period. The completed detector head, including ion chamber and electronics, was encapsulated in Hysol 6020 casting resin. A typical calibration curve for these detectors is given in Figure 2.2.

2.2.2 Residual Instrument System Recorder. The two-channel recorder used with this system consisted of an Esterline-Angus-chart drive to supply the time base and

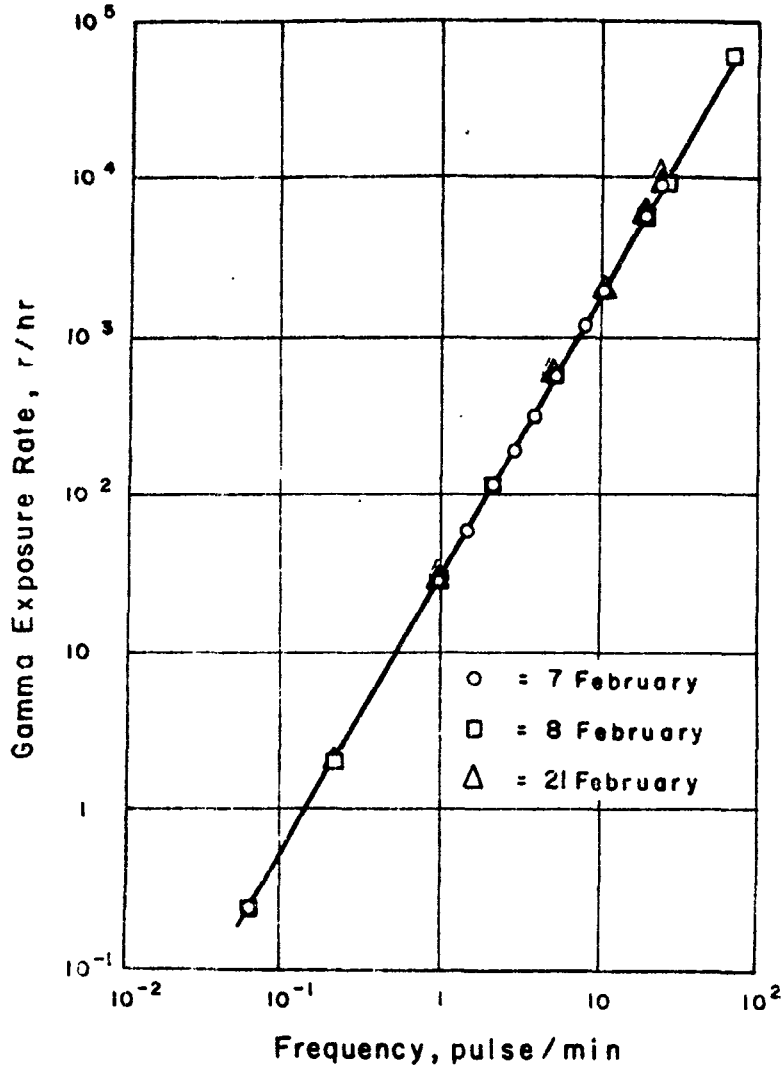


Figure 2.2 Graph showing a typical calibration curve for the Conrad detectors. These detectors were calibrated with the 200-curie $Co^{60}$ source and the 250-kv X-ray generator.

two electric styluses writing on Teledeltos paper charts. The output from the detector head was fed through an amplifier directly to Stylus No. 1, which produced a mark for each detector-output pulse. In addition, the detector output was fed to a scale-of-11 counter, thence to Stylus No. 2. Thus, Stylus No. 2 produced one mark for each 11 output pulses from the detector. In this manner, a chart speed slow enough for the required five-day operating period could be used while maintaing resolution of the fastest anticipated pulse-repetition rate. In operation, the record from Stylus No. 1 was used until

the pulse-repetition rate was so great that the recorded marks overlapped and could not be resolved. At that time, Stylus No. 2 would be used, with each mark representing 11 pulses from the detector head. The chart drive that supplied the time base was calibrated with a Watchmaster before each event. By means of the Watchmaster, the chart drive could be set to have a maximum error of 1 minute in 24 hours, or ±0.069 percent. This was not the optimum recording system for use with this detector but rather a compromise forced by a lack of funds and time.

2.2.3 Initial Instrument System, Gustave I Detector. For the high-range, fast-resolution detector, the basic circuit of Figure 2.1 was used with a scintillation detector as the sensing element. The latter consisted of an RCA 929 phototube and a National Radiac Scintillon Branch plastic phosphor mounted in an electron-equilibrium thickness of bakelite to provide an air-equivalent response (Reference 8). The purpose of the electron-equilibrium layer was to present a source of electrons that might be scattered into the crystal to replace those electrons produced by radiation absorbed near the crystal surfaces and lost without being detected. These detectors were constructed to cover three ranges: $10^2$ to $10^6$ r/hr, $10^3$ to $10^7$ r/hr, and $10^4$ to $10^8$ r/hr.

The overall detector response is given approximately by:

$$f = kr \tag{2.3}$$

Where: f = the pulse repetition rate

r = the gamma-exposure rate in r/hr

k = a parameter chosen to meet specific design objectives

The maximum pulse-repetition rate of these instruments was 1,000 pulses/sec, the maximum rate that could be resolved by the recorder (a Cook Research Laboratory MR-33 eight-channel magnetic-tape recorder). Typical calibrations for these detectors are shown in Figure 2.3. Figure 2.4 shows the energy dependence of the Scintillon-phosphor Gustave I detector, relative to $Co^{60}$ gamma radiation at a rate of 100 r/hr. To reduce the errors due to flutter and wow, a 1,000-cycle-time base was recorded on the tape simultaneously with the gamma-exposure-rate data. An American Time Products transistorized-frequency standard with an accuracy of ±0.02 percent was used to provide the time base.

2.2.4 Photomultiplier Feedback Circuit, Initial Instrument System. This system was essentially the same as that used during Operation Castle (Reference 2). The detecting element, a Scintillon phosphor 2.75 inches in diameter by 0.5 inch in height mounted in a bakelite block for electron equilibrium, was placed inside a blast-resistant housing at the top of a light pipe. The output of the crystal after passing through the light pipe was detected by an RCA 6199 photomultiplier tube. The photomultiplier tube was used in a 100-percent-feedback circuit which held the photo-multiplier-tube-anode current nearly constant, regardless of the incident light flux, by reducing the dynode voltage (Figure 2.5). The gain of a photomultiplier tube with constant anode current was approximately proportional to the antilog of the dynode voltage. In this manner, a useful dynamic range of about a factor of $10^7$ was realized.

2.2.5 Calibration. Three radiation sources (a 250-kv X-ray generator, a 2.5-Mev Van de Graaff generator, and a 200-curie $Co^{60}$ source) were used in the calibration of

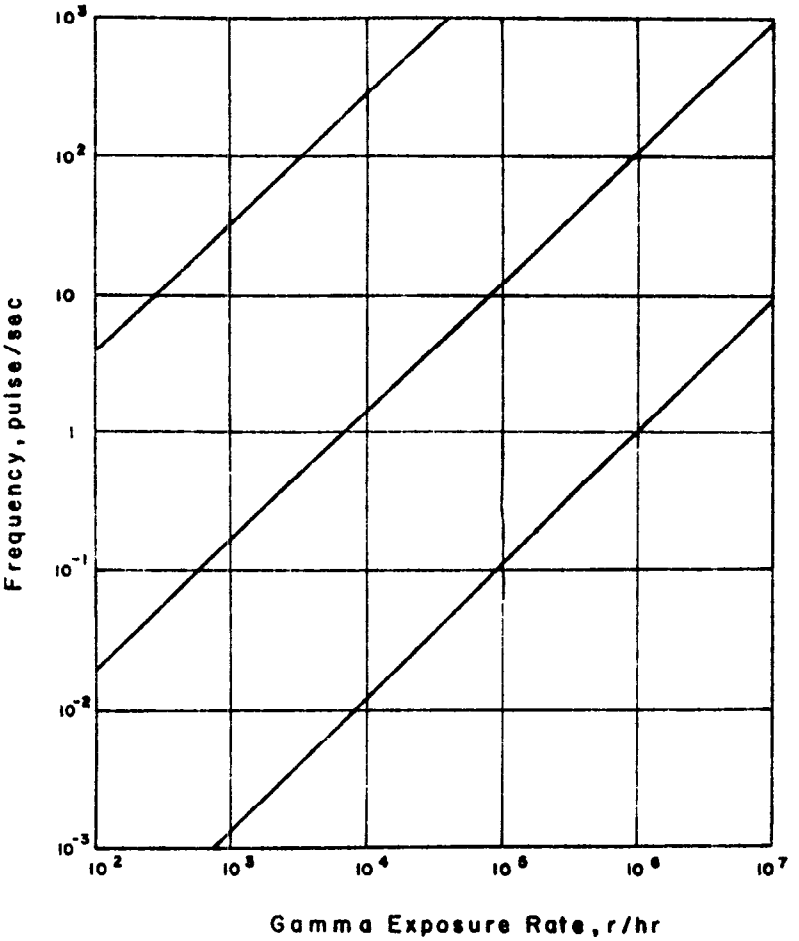


Figure 2.3 Graph showing typical calibration curves for the Gustave detectors. These detectors were calibrated with the 250-kv X-ray generator and the 2.5-Mev Van de Graaff generator.

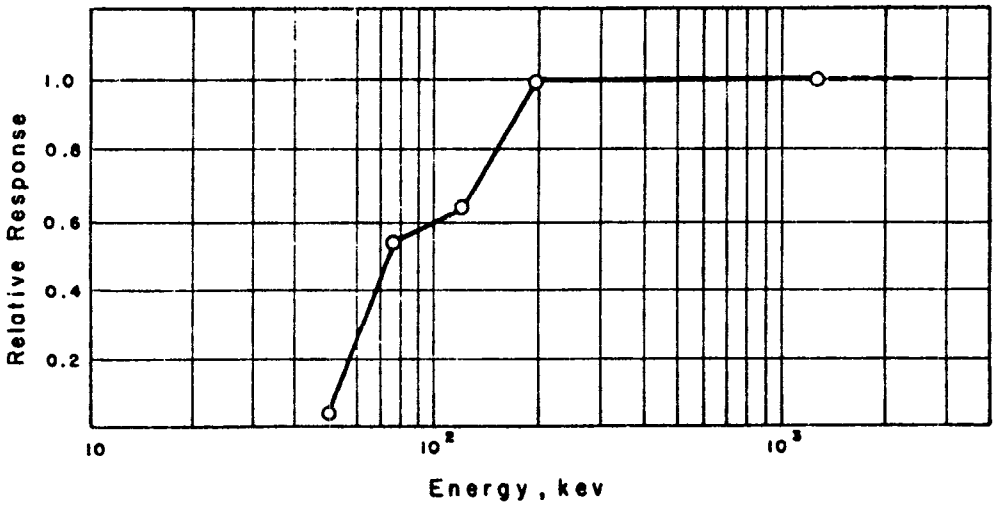


Figure 2.4 Energy dependence of Gustave I detector normalized to $Co^{60}$ energy (1.25 Mev), dose rate 100 r/hr.

the Project 2.2 instruments. The Conrad detectors were calibrated with the 200-curie $Co^{60}$ source and the 250-kv X-ray generator. The initial-gamma instruments, the Gustaves and the photomultiplier feedback-circuit detectors, were calibrated with the 250-kv X-ray and the 2.5-Mev Van de Graaff generator.

The 250-kv X-ray machine was operated at an applied potential of 250 kv, and 10-ma current. The X-ray beam was hardened with 1 mm of cadmium filtration to give an effective energy of 190 kev. The instrument response to this beam was the same as for $Co^{60}$, since the instrument response was flat to below 125 kev. The maximum

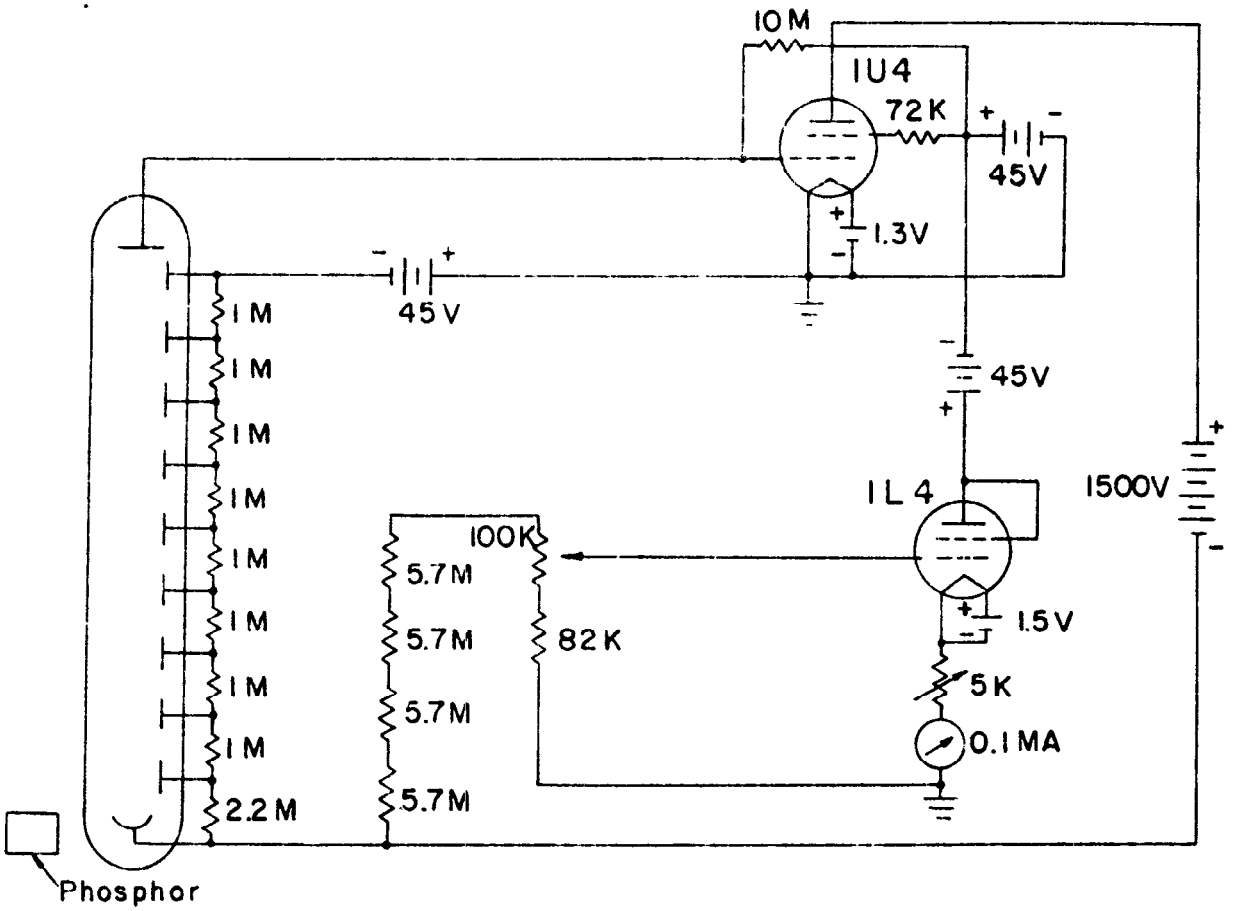


Figure 2.5 Schematic diagram showing the photomultiplier feedback circuit of the initial-gamma detector system.

usable-exposure rate attainable with this X-ray generator (consistent with good geometry) was 6,400 r/hr.

The Van de Graaff generator was operated at 1.0, 1.5, and 2.0 Mev, resulting in a maximum rate of $10^6$ r/hr.

The 200-curie field calibrator was specifically designed for operation under EPG weather conditions. The main components were the source container and the control trailer. The source container was made of stainless steel and the plug-and-rise-tube assembly of Monel metal. The source, inclosed in a double-walled Monel capsule, was raised and lowered pneumatically and was supported by three spring-loaded pins, one of which actuated a microswitch to indicate when the source was up.

The $Co^{60}$ was in pellet form and filled a space 0.39 inch in diameter and 1.58 inches in length. The Monel metal shielding (capsules and rise tube) was 0.33 inch. The

source was calibrated in the field over the exposure-rate region used with a set of Victoreen r-meters calibrated at National Bureau of Standards (NBS) in March 1956.

2.2.6 High-Range Initial-Gamma Station Calibration. There were no sources available for direct gamma-radiation calibration up to the maximum ranges of the initial-gamma instruments. Because of this lack, scintillation detectors were used, thereby enabling calibration with a light source. In practice, the instruments were directly calibrated by the use of the 200-curie $Co^{60}$ source in the field and a Van de Graaff generator in the laboratory to the limit of the available radiation rates. The calibration was then extended to the maximum range through the use of a light calibration, which was normalized to the radiation calibration.

The light calibrator consisted of a light source filtered to provide a beam having approximately the same spectral quality as the light output of the scintillator, and a series of neutral-density filters that varied the light output in known discrete steps. Errors due to the direct response of the circuit elements to gamma radiation were introduced into the calibration; however, these errors were shown to be small in the ranges where the light and radiation calibrations overlapped. There were no reasons why the relative error should have increased beyond the range of dual calibration.

## 2.3 READOUT ERROR AND ACCURACY OF THE GUSTAVE AND CONRAD SYSTEMS

In general, the output of the Gustave and Conrad detectors may be given as:

$$r = kt^n \tag{2.4}$$

Where: $r$ = gamma exposure rate

$t$ = time between output pulses

$n$, $k$ = design parameters

If the error in reading time between pulses (i.e. time base) is $\Delta t$, then:

$$r + \Delta r = k(t + \Delta t)^n$$

$$\Delta r = k\left[(t + \Delta t)^n - t^n\right]$$

$$\frac{\Delta r}{r} = \frac{(t + \Delta t)^n - t^n}{t^n} \tag{2.5}$$

For $\frac{\Delta t}{t} \ll 1$, this formula reduces to the definition of differentials.

$$\frac{\Delta r}{r} \doteq \frac{n\Delta t}{t} \tag{2.6}$$

Where: $\frac{\Delta r}{r}$ = the relative error in gamma-exposure rate due to errors in the time measurement

$\frac{\Delta t}{t}$ = the relative time-measurement error

For the Conrad I detector, n = -2, and:

$$\frac{\Delta r}{r} \doteq \frac{-2\Delta t}{t} \tag{2.7}$$

In practice, at high-pulse-repetition rates, a number of pulses N over a period T were used to read out the data. Hence, from equation 2.5:

$$\frac{\Delta r}{r} \doteq \frac{(Nt + \Delta t)^n - (Nt)^n}{(Nt)^n}$$

$$\frac{\Delta r}{r} \doteq \frac{(T + \Delta t)^n - (T)^n}{T^n} \tag{2.8}$$

$$\doteq \frac{n\Delta t}{T}$$

Where: $\Delta t$ now includes all errors in reading the time interval T.

The time-base error for the Conrad recorders was ± 0.069 percent; therefore, the readout error was negligible, and the errors of the Conrad I system (of the order of 10 percent) could be attributed to the detector itself.

For the Gustave I system, n ≐ -1, and:

$$\frac{\Delta r}{r} \doteq \frac{-\Delta t}{T} \tag{2.9}$$

Hence the Gustave I system error was essentially that of the detector (the time-base error ± 0.02 percent), and was of the order of 10 percent.

## 2.4 BEACH-BALL-RADIATION-DETECTOR-TELEMETER UNIT

To attain the objective of measuring the residual-exposure rate on the crater of a land-surface burst, a droppable radiation-detector-telemeter unit was devised. A Gustave I detector system was connected to key a ½-watt VHF transmitter that had been constructed in the field. The detector and transmitter were mounted in a polyethylene bottle suspended at the center of an air-inflated, 5-foot, plastic beach ball. The beach ball was attached to a 27-pound lead brick by means of a 6-foot line. This made it possible to drop the system from a helicopter more accurately with a minimum of impact shock to the instrumentation. The lead brick hit the ground first and allowed the beach ball to slow down over the 6-foot distance before hitting the ground. In addition, the beach ball itself acted as a good impact absorber. Once the beach ball was released, the helicopter could go a short distance away and orbit in a radiologically safe region, while receiving the data transmitted from the beach-ball unit.

## 2.5 THERMAL-RADIATION DETECTOR

The thermal-radiation detector consisted of a phototube, amplifier, and high- and low-band-pass filters. The phototube output was produced by incident-thermal radiation from a nuclear device, lightning strokes, or other sources. This output was fed to a high band-pass filter that passed only signals with a rise time similar to those caused by nuclear detonations and to a low band-pass filter that passed only those signals with a duration typical of nuclear detonations. Thus, an incident thermal-radiation signal had to have both a rise time and a duration typical of nuclear devices in order to activate the thermal-radiation detector.

# Chapter 3
# RESULTS and DISCUSSION

## 3.1 RESIDUAL-RADIATION MEASUREMENTS

The data obtained from the residual-radiation stations are shown in Figures 3.1 through 3.18 in the form of log-log plots for convenience of presentation and for ease of determination of the decay exponent. The decay exponent was equal to the slope of a straight line drawn through the data points that were considered to be related to each other only by radioactive decay. All residual data was analyzed in detail for this report. The instruments for those stations represented by Figures 3.3, 3.11, and 3.12 were operating at levels below their high-resolution region and did not yield the essentially continuous curves shown in the remainder of the group of Figures 3.1 through 3.18. On Figures 3.1 through 3.18 the slopes are shown as dashed lines which were drawn through the linear portion of the curves. In drawing these dashed lines, early times were avoided when the concentration of gamma-ray sources was still building up because of continuing deposition of fallout material, and other data points were ignored in cases where rain or wind had redistributed the fallout material and caused perturbations in the decay curve.

Measured residual-gamma-radiation doses for each of the four shots are plotted on maps of Bikini Atoll in Figures 3.19 through 3.22. Free-field exposures shown on these figures were extrapolated to infinite time using Equation 1.1, Section 1.3.2, of this report.

Tables 3.1 through 3.4 summarize the data on residual-station locations, time of arrival of fallout, maximum-observed-exposure rate, total exposure, and decay exponent. The average decay exponent was found to be 1.1 for Shots Zuni and Tewa, neglecting the results from Station 221.04C, which received too little exposure for accurate evaluation). In the many cases where there was early rain leaching, the slope indicated by the data points taken after rain had ceased was used to help determine the best-fit straight line.

In these curves, the gamma-exposure rate after rainfall was approximately half of that expected if the normal radioactive decay were the only cause of change of exposure rate.

In Figures 3.3 and 3.18, the buildup of the exposure rate was apparently more complex than the monotonic buildup presented by most of the other figures. It appears that fallout ceased to arrive for a short period at 60 minutes (in Figure 3.18) and then began to arrive again.

Slope changes are evident in the curves in Figures 3.9 and 3.10 after about +500 minutes. This effect was probably not due to instrumentation errors because these curves represented the data from two independent instruments located at the same station. A possible explanation of these slope changes was the presence of one (or more than one) radioactive isotope whose half life was such that the decay was slower than the combined fission fragment decay of $t^{-1.2}$, and the decay slope was dominated by this isotope from about +500 minutes until the end of the record. However, the instrumen-

tation did not record for a sufficiently long time to determine definitively the half life of this isotope.

Reliability of Residual-Radiation Data. In general, the residual instrumentation functioned either well or not at all. Tables 3.1 through 3.4 show that the major malfunctions were due to inoperative chart drives. The possibility of malfunc-

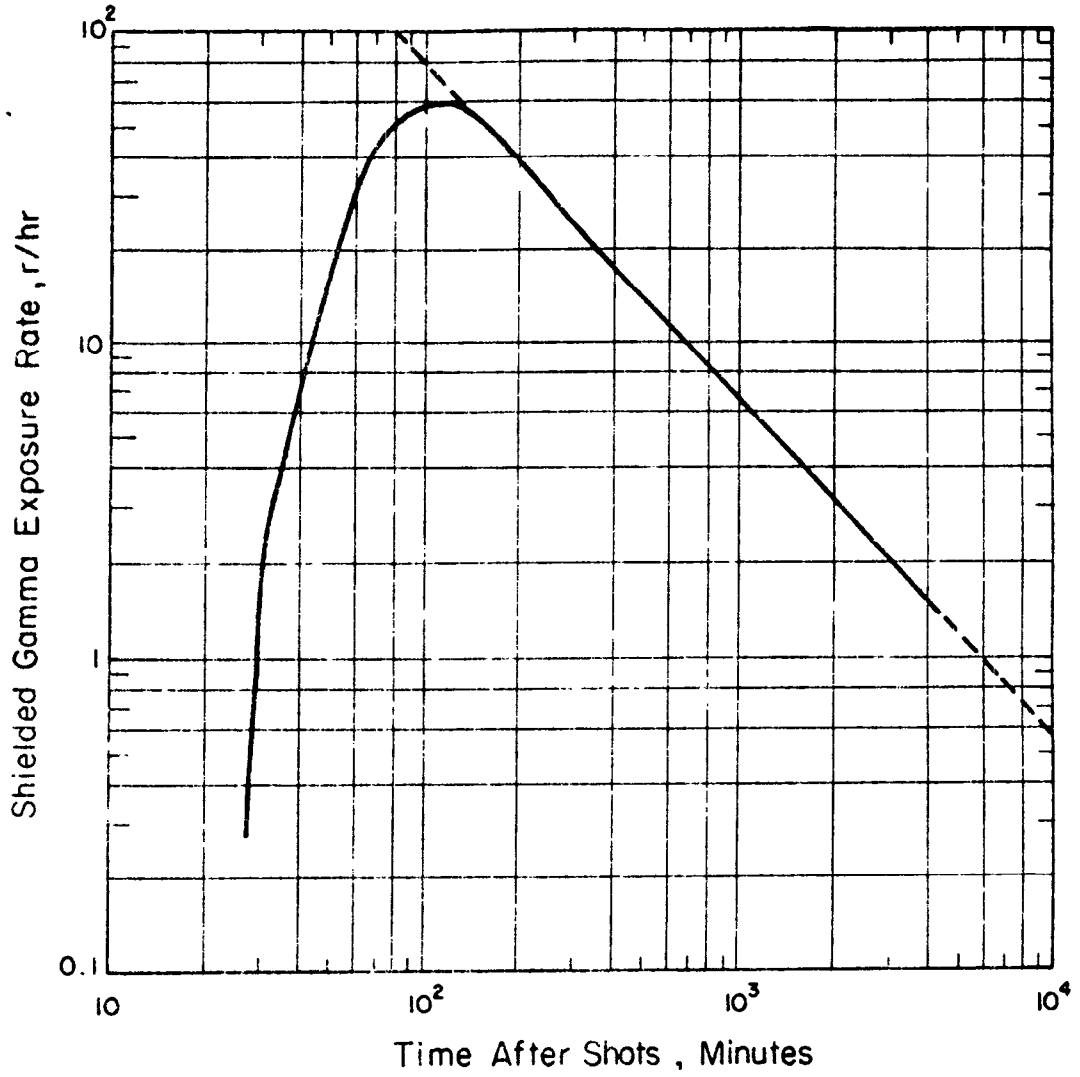


Figure 3.1 Residual exposure rate within blast shield versus time for Shot Zuni; Station 221.03, range 68,600 feet. For unshielded rate multiply by 1.4. Total 72.9-hour exposure, 502r.

tioning of the recorders was anticipated prior to the operation; however, lack of funds and time forced the use of these recorders. The recorders that worked were checked with a Timemaster and adjusted to within ±0.069 percent accuracy. The repeated calibrations of the instrument systems indicated a maximum total error of less than 10 percent.

Figures 3.1, 3.3, 3.7, 3.8, 3.9, 3.13, 3.14, 3.15, 3.16, 3.17, and 3.18 present data taken with the detector heads inside a steel pipe which served as blast and thermal protection. The results from these stations should be increased by a factor of about 1.4 to compensate for the shielding of the blast housings. This estimate of the shielding



Text continued on Page 43.

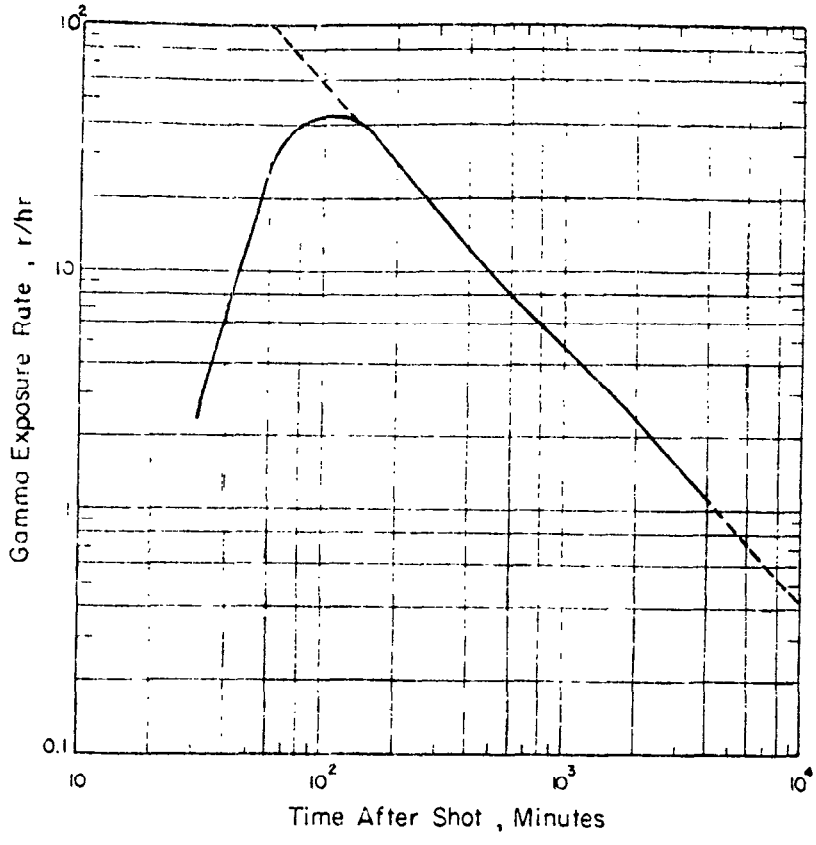


Figure 3.2 Unshielded residual exposure rate versus time for Shot Zuni; Station 221.06, range 70,900 feet. Total 77.8-hour exposure, 349r.

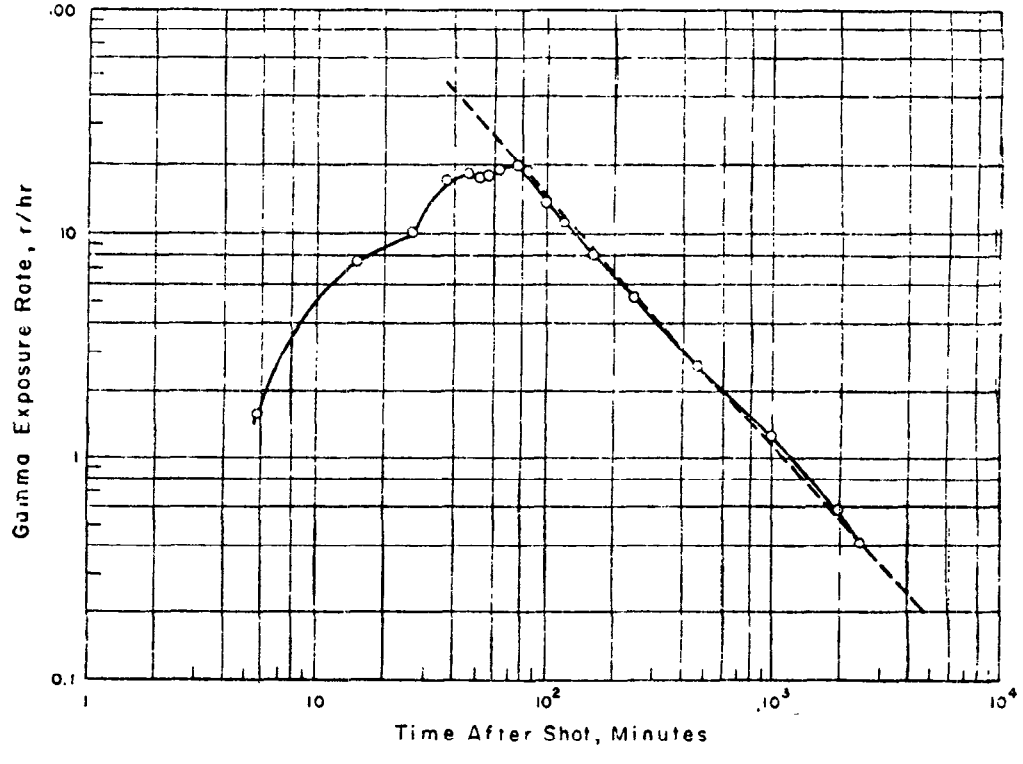


Figure 3.3 Residual exposure rate versus time for Shot Zuni; Station 221.01C, range 10,300 feet. For unshielded rate multiply by 1.4. Total 85-hour exposure, 99r.

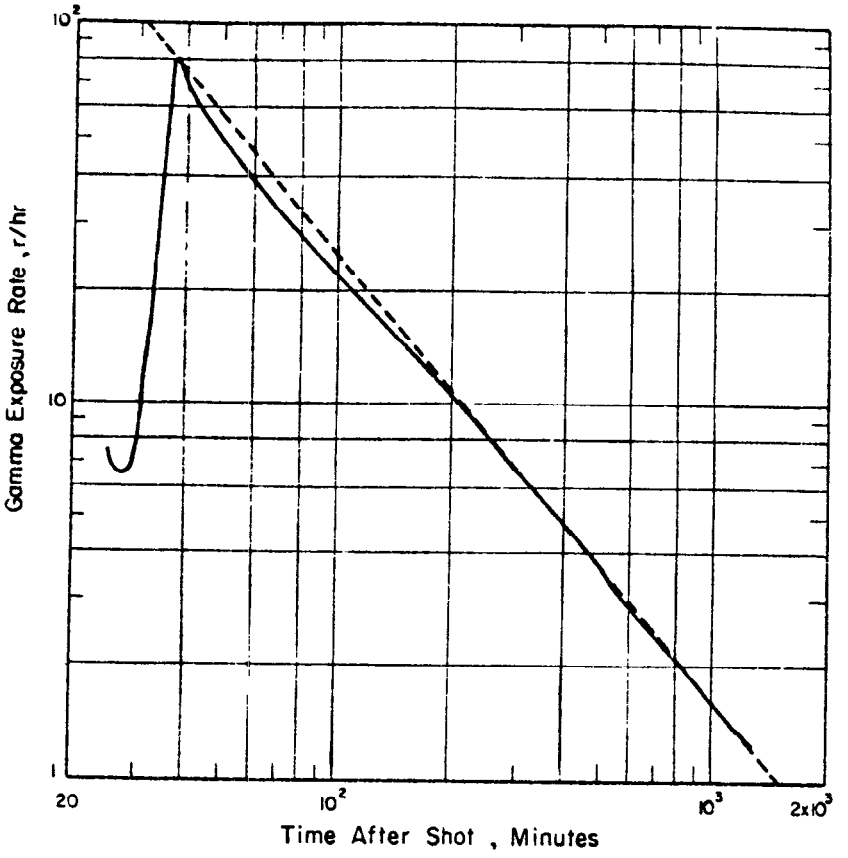


Figure 3.4 Unshielded residual exposure rate versus time for Shot Zuni; Station 221.02C, range 43,400 feet. Total 20.4-hour exposure, 125r.

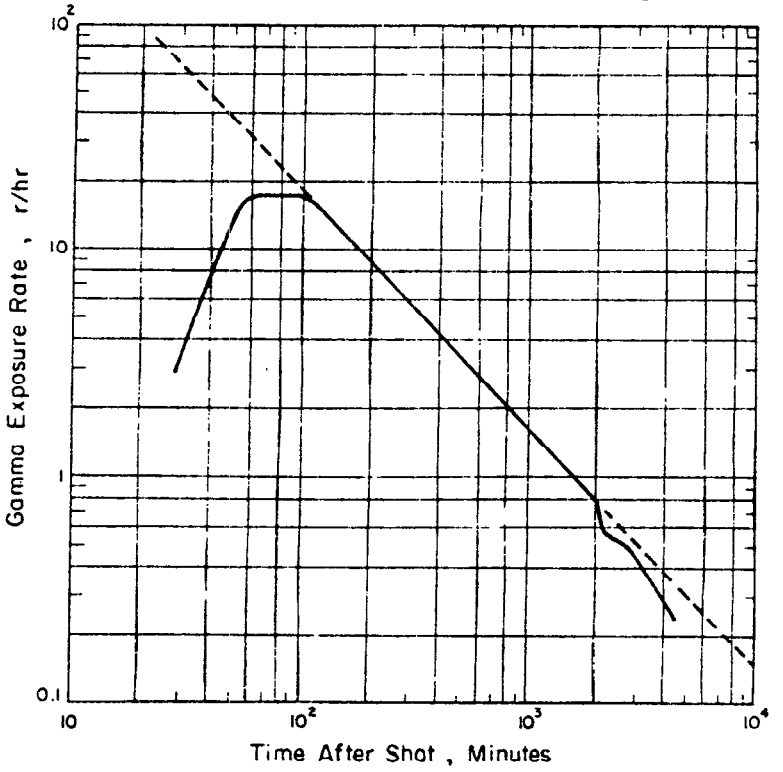


Figure 3.5 Unshielded residual exposure rate versus time for Shot Zuni; Station How, range 78,000 feet. Total 74.5-hour exposure, 126r.



Pgs. 32 thru 36 Deleted.

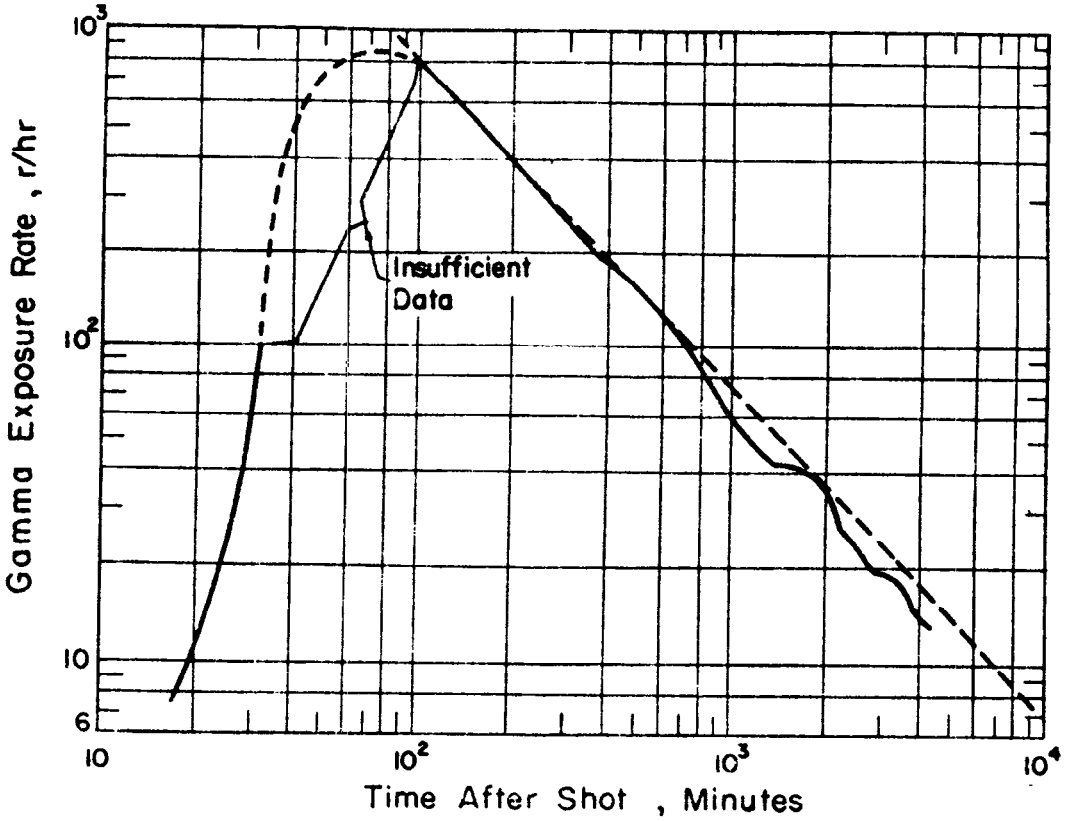


Figure 3.16 Residual exposure rate versus time for Shot Tewa; Station 221.01, range 28,950 feet. For unshielded rate, multiply by 1.4. Total 74.8-hour exposure, 3,055r.

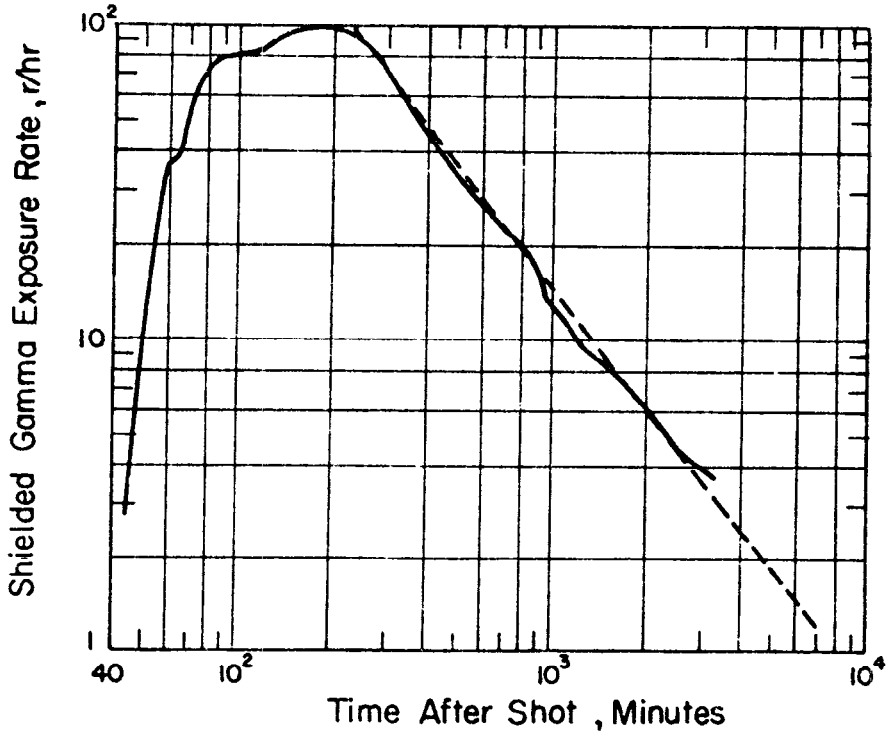


Figure 3.17 Residual exposure rate within blast shield versus time for Shot Tewa; Station 221.03, range 17,550 feet. For unshielded rate, multiply by 1.4. Total 55-hour exposure, 948r.

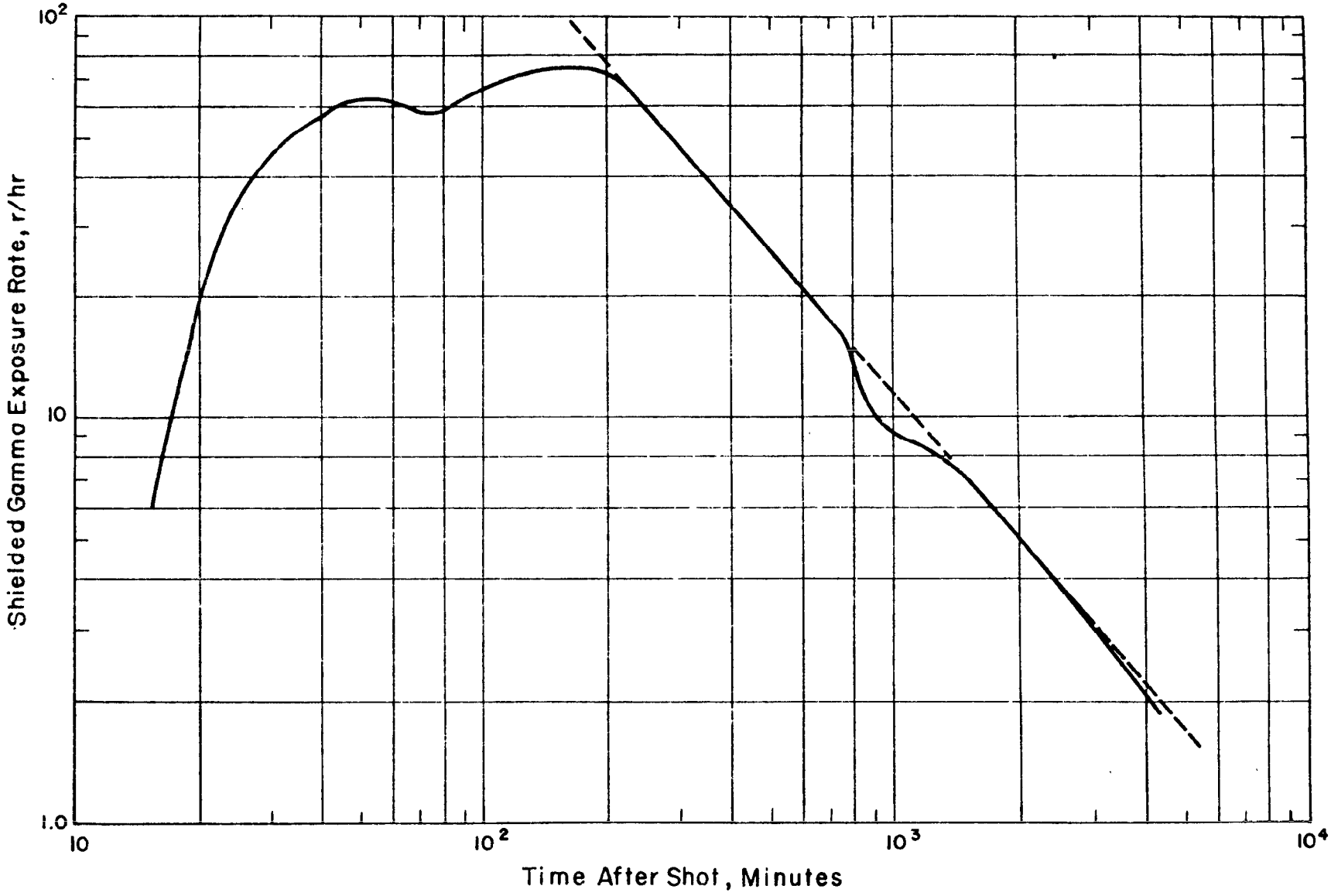


Figure 3.18 Residual exposure rate within blast shield versus time for Shot Tewa; Station 221.04, range 22,220 feet. For unshielded rate, multiply by 1.4. Total 73-hour exposure, 814r.

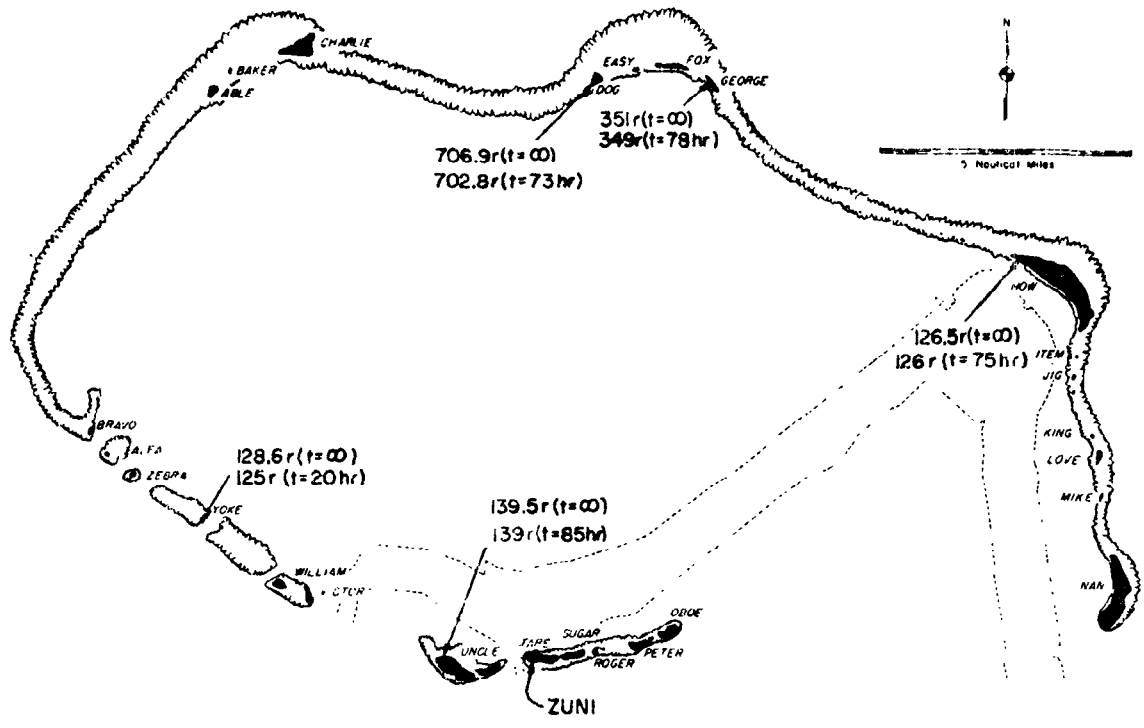


Figure 3.19 Map of Bikini Atoll showing unshielded residual exposures fot Shot Zuni. This illustration gives exposures at Islands Dog, George, How, Uncle, and Yoke. See Table 3.1 for references to station designations, distances from ground zero, arrival times, and maximum exposure rates.

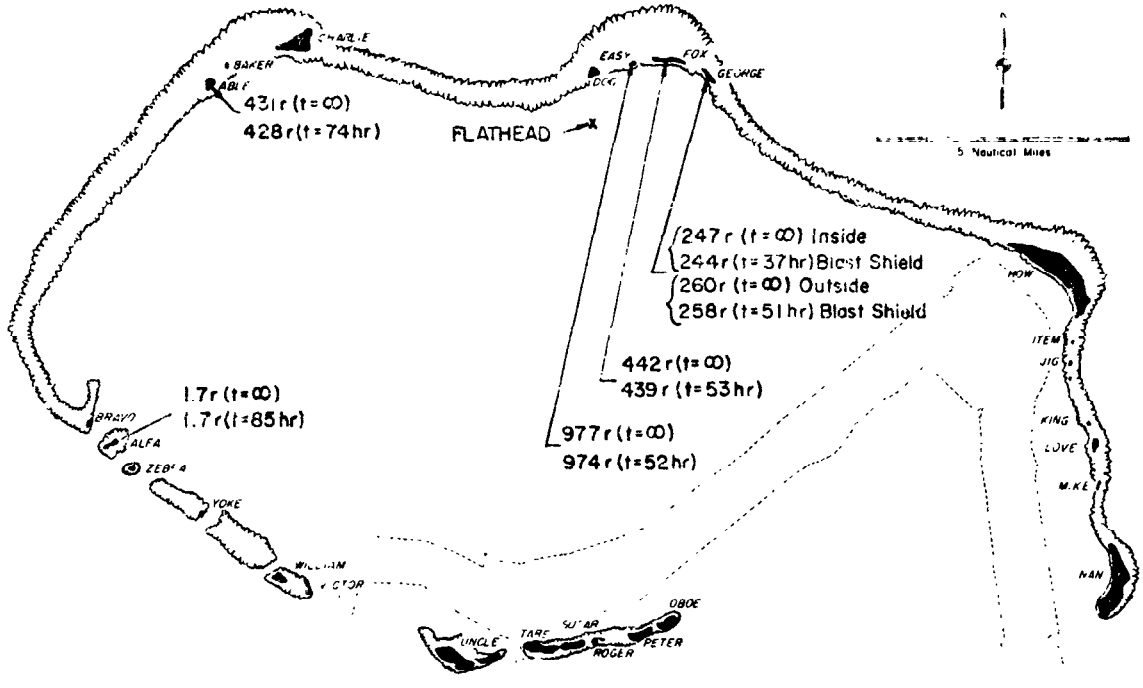


Figure 3.20 Map of Bikini Atoll showing unshielded residual exposures for Shot Flathead. This illustration gives exposures at Islands Able, Alfa, Easy, Fox, and George (a and b). See Table 3.2 for references to station designations, distances from ground zero, arrival times, and maximum exposure rates.

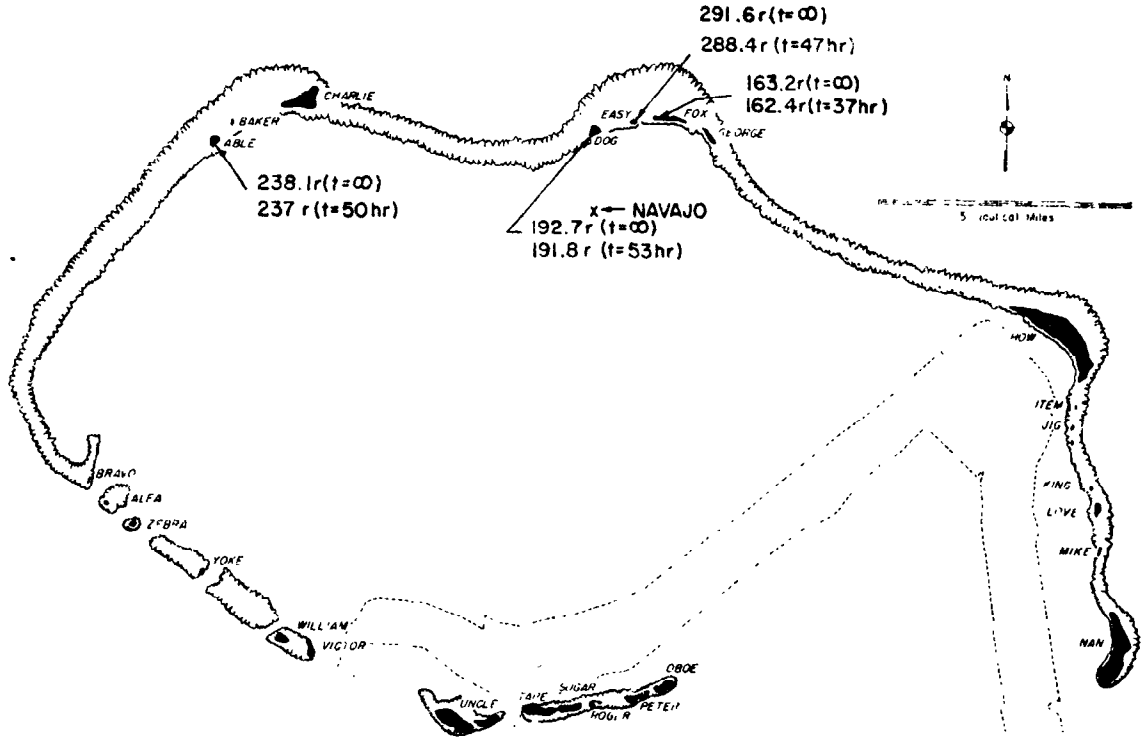


Figure 3.21 Map of Bikini Atoll showing unshielded residual exposures for Shot Navajo. This illustration gives exposures at Islands Able, Dog, Easy, and Fox. See Table 3.3 for references to station designations, distances from ground zero, arrival times, and maximum exposure rates.

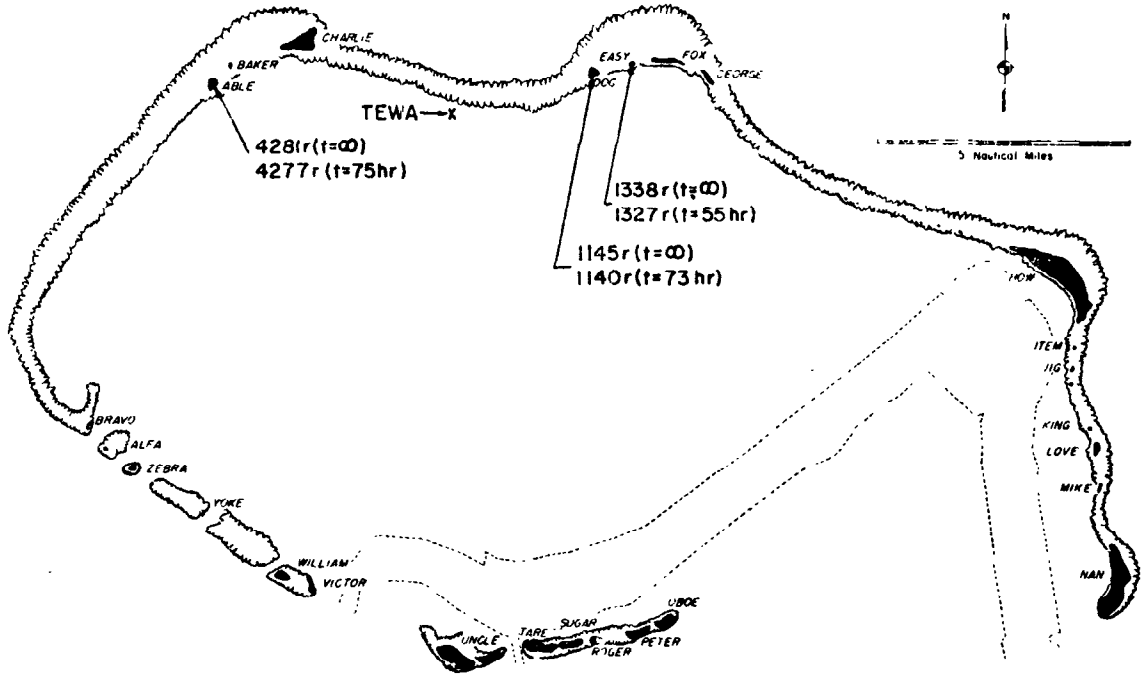


Figure 3.22 Map of Bikini Atoll showing unshielded residual exposures for Shot Tewa. This illustration gives exposures at Islands Able, Dog, and Easy. See Table 3.4 for references to station designations, distances from ground zero, arrival times, and maximum exposure rates.

TABLE 3.1 SHOT ZUNI INSTRUMENTATION AND RESIDUAL-EXPOSURE INFORMATION

| Island | Station | Azimuth From Ground Zero | Distance From Ground Zero | Arrival Time | Maximum Rate* | Total Exposure* | Decay Exponent |
|---|---|---|---|---|---|---|---|
| | | degree | ft | minute | r/hr | r | |
| Dog | 221.03 | 5.5 | 68,600 | 27.7 | 81.2 | 703(72.9 hr) | 1.07 |
| George | 221.06 | 17.1 | 70,900 | 31 | 42 | 349(77.8 hr) | 1.07 |
| How | Portable | 60 | 78,000 | 28.8 | 17 | 126(74.5 hr) | 1.04 |
| Uncle | 221.01C | 268.8 | 10,300 | 2 6 | 28 | 139(85 hr) | 1.1 |
| Yoke | 221.02C | 292.2 | 43,400 | 25.3 | 80 | 125(20.4 hr) | 1.18 |
| Nan | Portable | No fallout | | | | | |
| Charlie | 221.02 | Drive inoperative | | | | | |
| Love | Portable | Stylus and drive inoperative | | | | | |
| Oboe | 220.08C | Drive inoperative | | | | | |
| Peter | 220.14C | Stylus inoperative | | | | | |
| Roger | 220.09C | Stylus and drive inoperative | | | | | |
| William | 221.01C | Drive inoperative | | | | | |
| Alfa | 221.04C | Drive inoperative | | | | | |

* Corrected to free-field values.

TABLE 3.4 SHOT TEWA INSTRUMENTATION AND RESIDUAL-EXPOSURE INFORMATION

| Island | Station | Azimuth From Ground Zero | Distance From Ground Zero | Arrival Time | Maximum Rate* | Total Exposure* | Decay Exponent |
|---|---|---|---|---|---|---|---|
| | | degree | ft | minute | r/hr | r | |
| Able | 221.01 | 280.8 | 28,950 | 17.5 | 1,078 | 4,277(74.8 hr) | 1.03 |
| Dog | 221.03 | 76.7 | 17,550 | 44.7 | 140 | 1,327(55 hr) | 1.29 |
| Easy | 221.04 | 75.2 | 22,220 | 15.3 | 105 | 1,139.6 (73 hr) | 1.11 |
| Oboe | 220.08C | No fallout | | | | | |
| How | Portable | Stylus inoperative | | | | | |
| Fox | 221.05 | Drive inoperative | | | | | |
| William | 221.01C | Drive inoperative | | | | | |
| Yoke | 221.02C | Drive inoperative | | | | | |

* Corrected to free-field values.

factor was derived from the field measurements at station 221.06, Shot Flathead, where one detector was inside and the other was outside the blast housings. On the other hand, Figures 3.2, 3.4, 3.5, 3.6, 3.10, 3.11, and 3.12 present data from detector heads without blast shields. These detectors were calibrated for free-field conditions ($Co^{60}$) and gave free-field data.

## 3.2 INITIAL-RADIATION MEASUREMENTS

The results from the initial-gamma stations are shown in Figures 3.23, 3.24, and 3.25. The initial-gamma station for Shot Zuni (Station 220.09C) was destroyed by the

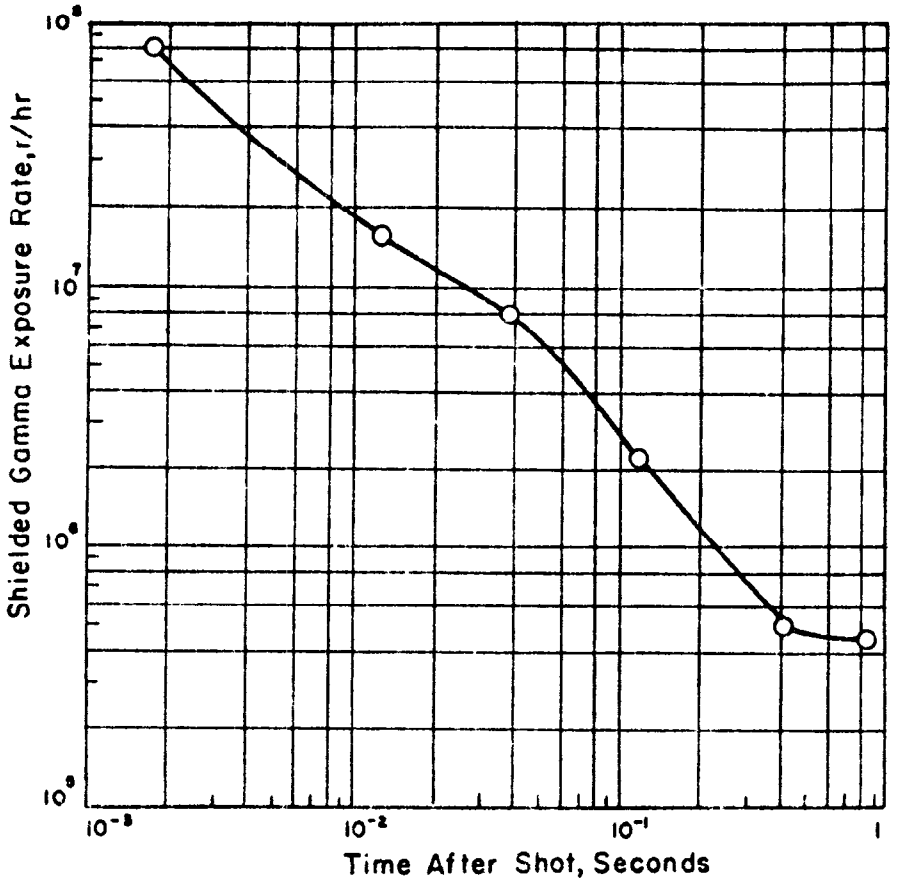


Figure 3.23 Shielded initial exposure rate versus time for Shot Zuni; Station 220.09C, range 7,000 feet. For unshielded rate multiply by 1.2.

shock wave, and the data from this station were available only to shock arrival and are given in Figure 3.23. Figures 3.26, 3.27, and 3.28 present the total-initial-gamma exposure as a function of time.

The initial-gamma-exposure-rate data presented are subject to uncertainty in absolute magnitude. Data reduction indicated a strong possibility that the wiring of the magnetic-tape recorders might not have been the same as previously presumed and that the association of a particular recorder channel with a particular-detector-sensitivity range might have been incorrect. The wiring could not be checked in the laboratory because the equipment had been disassembled at the termination of the field phase of the operation. Subsequent analysis of the recorded pulse shapes has led to the association assumed for the initial-gamma data presented herein, and the derived total-exposure values agreed reasonably well with those measured by Operation Redwing

 Pgs 44 thru 45 Deleted

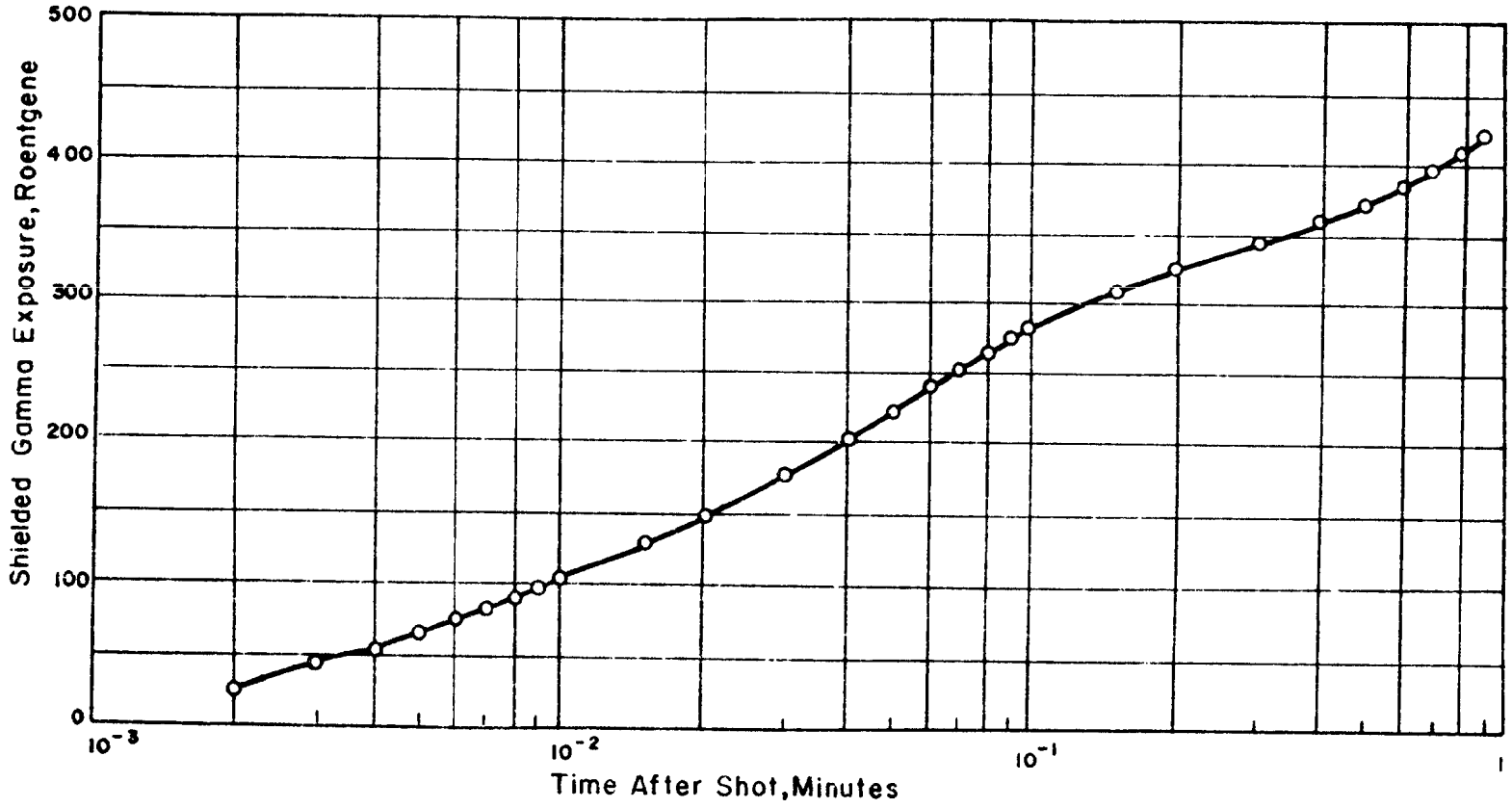


Figure 3.26 Shielded initial exposure versus time for Shot Zuni; Station 220.09C, range 7,000 feet. For unshielded exposure multiply by 1.2.

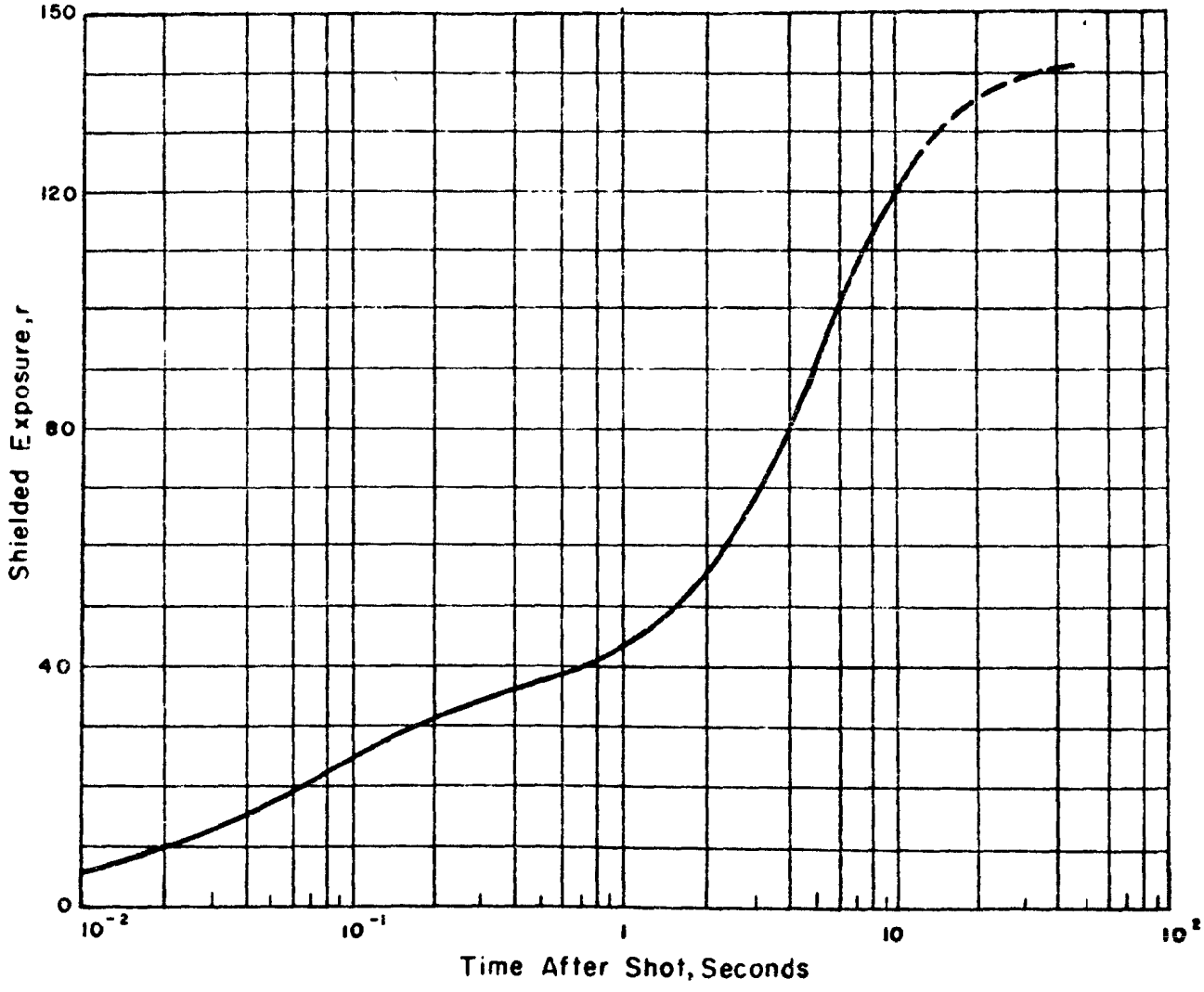


Figure 3.27 Shielded initial exposure versus time for Shot Flathead; Station 221.04, range 7,730 feet. For unshielded exposure multiply by 1.2.

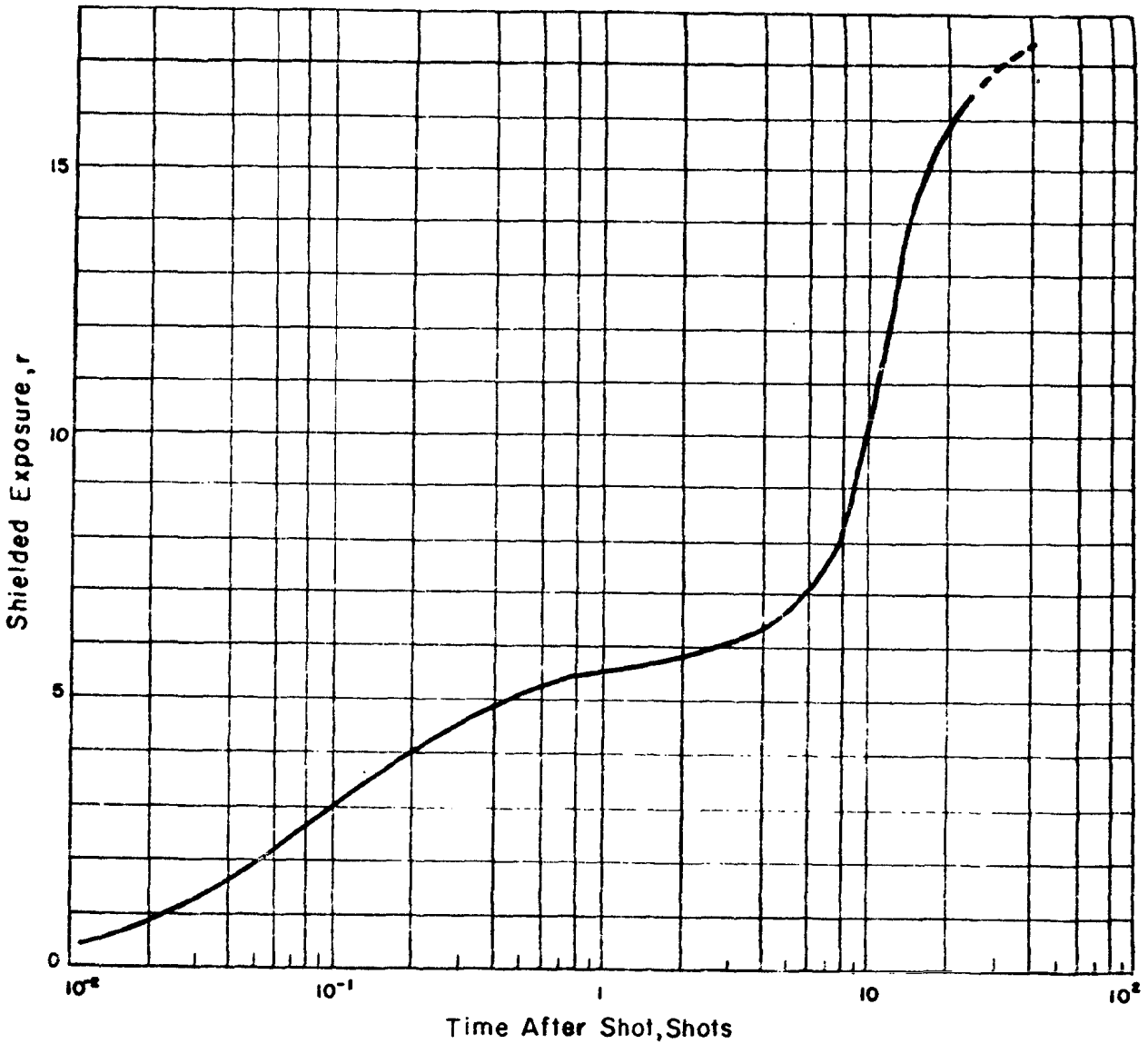


Figure 3.28 Shielded initial exposure versus time for Shot Navajo; Station 221.05, range 13,170 feet. For unshielded exposure multiply by 1.2.

Project 2.1 (Reference 9). However, there is still some uncertainty on this point, and the curves presented may be off in absolute magnitude, although the shape of the curves as a function of time is probably correct.

The initial-gamma values given represent those observed at the detector and should be multiplied by a factor of approximately 1.2 to correct for station shielding. This factor of 1.2 is a measured value of the attenuation of the blast shield for $Co^{60}$ radiation; the attenuation is a function of the energy of the incident radiation. Time is a factor only in that after one minute there is little gamma radiation in this energy range ( >1 Mev). Figures 3.23 through 3.28 should be multiplied by 1.2 to give free-field values.

The data in Figure 3.26 is in reasonable agreement with similar data in Reference 9, especially after the data of Figure 3.26 has been extrapolated to a time equivalent to that reported by Operation Redwing Project 2.1.

Figures 3.27 and 3.28 show that approximately $^2/_3$ of the total-initial exposure for Shot Flathead 221.04 and Shot Navajo 221.05 was delivered after the arrival of the shock front. Most of this exposure was due to the enhancement caused by the hydrodynamic effect because the exposure rate was decaying rapidly before the arrival of the shock front.

Reference 9 compares measured-initial-gamma exposure-versus-distance curves with curves computed from TM 23-200. For the purpose of comparison with published data, integrated-initial-gamma-rate data from Figures 3.26, 3.27, and 3.28 of this report have been plotted on the corresponding curves from Reference 9. In addition, extrapolation of Project 2.2 measured data (integrated-initial-gamma rate) to include initial-gamma dose delivered after the end of project records has been made using information and methods in Reference 10. Exposure received prior to start of project records has been neglected, since the exposure was relatively insignificant. The above-mentioned plots for Shot Zuni are shown in Figure 3.29 and for Shots Flathead and Navajo in Figure 3.30.

## 3.3 BEACH-BALL MEASUREMENTS

The objective of measuring the exposure rate at the lip of the crater from Shot Zuni was assumed by Project 2.2 at a late stage in the preparations for Operation Redwing. The beach-ball instrument was dropped onto the Shot Zuni crater lip at H + 6 hours. The fall apparently caused a change in the calibration of the system, because the received data indicated an exposure rate as high as 50,000 r/hr at this late time. Furthermore, rotor interference made reception of the transmitted signal difficult.

## 3.4 THERMAL-RADIATION DETECTOR

The thermal-radiation detector was installed on Site Nan for Shot Tewa at a range of approximately 20 miles, and the detonation was satisfactorily detected.

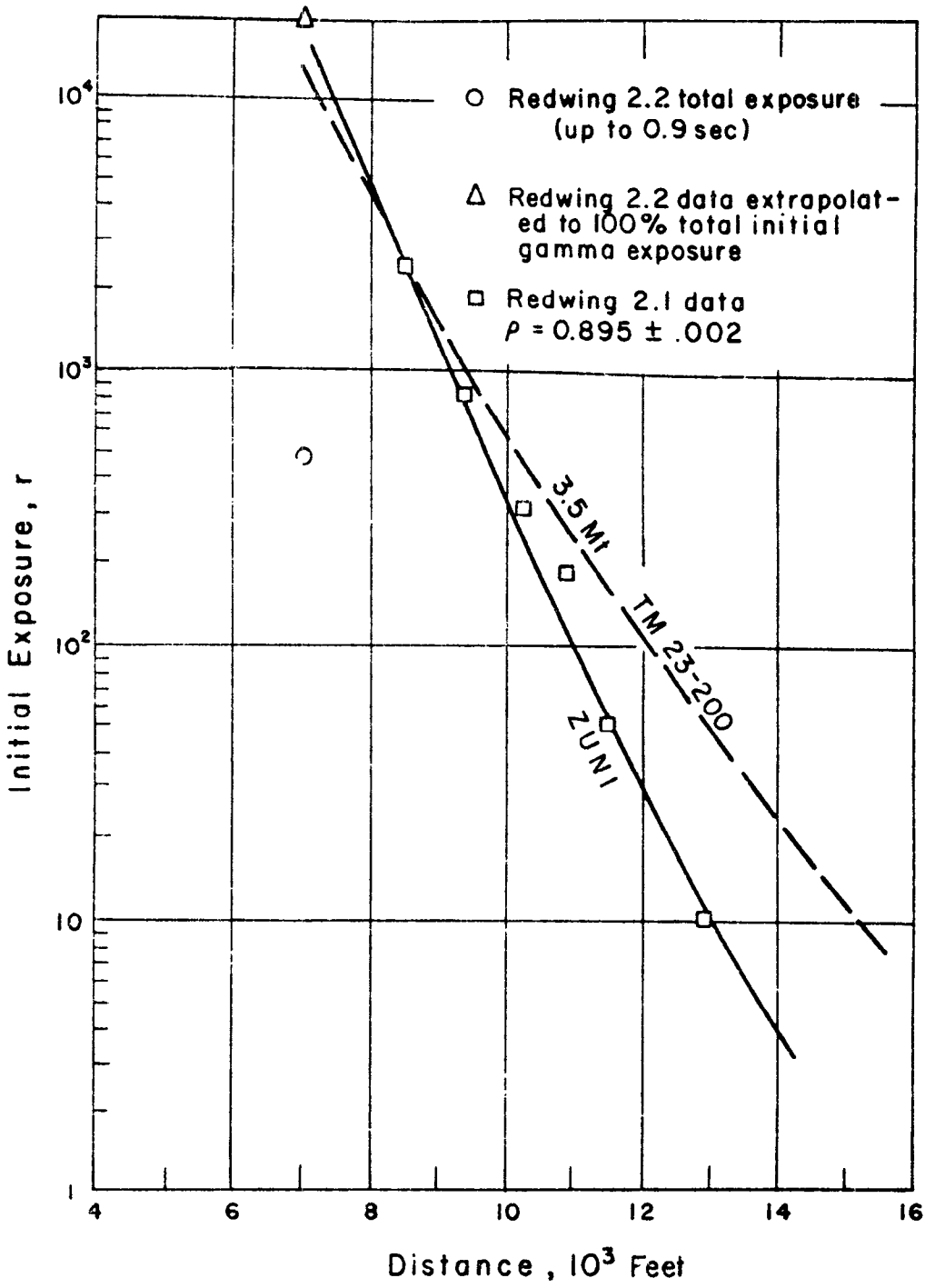


Figure 3.29 Shielded initial exposure versus distance, Projects 2.1 and 2.2, Shot Zuni. (Data from Redwing Project 2.2 plotted on curves presented in Redwing 2.1 WT report, Reference 9).

Pg. 51 Deleted.

# Chapter 4
# CONCLUSIONS

## 4.1 RESIDUAL-GAMMA-EXPOSURE RATE

The results of the residual-gamma-exposure-rate measurements showed that for some devices the decay exponent varied with both the type of device and the station location. The decay exponent was fairly uniform for different station locations for Shot Zuni (1.04 to 1.18) and rather variable for various station locations for Shot Navajo (1.07 to 1.39). Although no special significance was attached, the spread of values for the decay exponent seemed to be greater when the average value was high and smaller when the average value was low.

The residual-instrumentation system performed at about 50 percent of its capability. This was explained by the failure of the recorders, which were not designed as field instruments and were used because no others were available. There were no known failures of the Conrad detectors.

## 4.2 INITIAL-GAMMA-EXPOSURE RATE

Figures 3.27 and 3.28 show that approximately $^2/_3$ of the total-initial-gamma exposure was delivered after the arrival of the shock front. Insufficient initial-gamma rate or dose data was available to allow independent comparison with published scaling laws. Figures 3.29 and 3.30 indicate reasonable agreement of both Redwing Projects 2.1 and 2.2 data points with TM 23-200; however, measured dose-versus-distance curves exhibit a steeper slope than shown on Figure 4-3, page 4-12 of TM 23-200, thus indicating substantial deviations at short and very long ranges.

## 4.3 BEACH-BALL OPERATION

This experiment demonstrated the operational feasibility of using the beach-ball technique to drop a radiological telemeter onto a contaminated area.

## 4.4 THERMAL-RADIATION DETECTOR

The thermal-radiation detector operated satisfactorily for a 5-Mt detonation at a distance of 20 miles.

## 4.5 RECOMMENDATIONS

Because of experience gained by Project 2.5 during Operation Plumbbob, it is recommended that this experiment, with improved instrumentation, be repeated on other high-yield events, especially high-yield air bursts.

# REFERENCES


1. J. S. Malik; "Gamma Radiation Versus Time"; Projects 5.1 and 5.2, Operation Ivy, WT-634, November 1952; Los Alamos Scientific Laboratory, Los Alamos, New Mexico; Secret Restricted Data.

2. P. Brown and G. Carp; "Gamma Rate Versus Time"; Project 2.2, Operation Castle, ITR-913, May 1954; Signal Corps Engineering Laboratories, U. S. Army, Fort Monmouth, New Jersey; Secret Restricted Data.

3. Super-Effects Handbook; AFSWP 351, May 1952; Secret Restricted Data.

4. T. E. Petriken; "Evaluation of a Radiological Defense Warning System (Project Cloudburst)"; Project 6.1.1b, Operation Teapot, WT-1112, August 1957; Evans Signal Laboratory, Fort Monmouth, New Jersey; Secret Restricted Data.

5. M. G. Schorr and E. S. Gilfillan; "Predicted Scaling of Radiological Effects to Operational Weapons"; Project 2.0, Operation Jangle, WT-391, 15 June 1952; Technical Operations Incorporated, Arlington, Massachusetts; Secret Restricted Data.

6. D. C. Borg and C. Eisenhauer; "Spectrum and Attenuation of Initial Gamma Radiation from Nuclear Weapons, AFSWP 502B, January 1955"; Weapons Effects Division; Secret Restricted Data.

7. J. S. Malik; "Summary of Information on Gamma Radiation from Atomic Weapons; LA-1620, January 1954; Los Alamos Scientific Laboratory, Los Alamos, New Mexico; Secret Restricted Data.

8. R. T. Carr and G. J. Hine; "Gamma Ray Dosimetry with Organic Scintillators"; Nucleonics, November 1953; Unclassified.

9. P. Brown and others; "Gamma Exposure Versus Distance"; Project 2.1, Operation Redwing, Draft manuscript WT-1310, July 1957; U. S. Army Signal Research and Development Laboratory, Fort Monmouth, New Jersey; Secret Restricted Data.

10. "The Nuclear Radiation Handbook", AFSWP-1100, 25 March 1957; Nuclear Development Corporation of America, White Plains, New York; Secret Restricted Data.